Chapter 4

Analysis of Level Density Data for fp-Shell Nuclei: Systematic Calculations Using SAT-LSS

4.1 Preview

Level density calculations for 8 fp-shell nuclei $\{^{55}_{25}Mn_{30}, ^{56}_{26}Fe_{30}, ^{59}_{27}Co_{32}, ^{60}_{27}Co_{33}, ^{60}_{28}Ni_{32}, ^{62}_{28}Ni_{34}, ^{63}_{29}Cu_{34}, ^{65}_{29}Cu_{36}\}$ are carried out using SAT-LSS and the results are described in this chapter. The various conditions that led to the selection of the above eight nuclei are given in Sect. 4.2.1. In order to proceed with the calculations, one needs to have a reference energy, a set of s.p. orbits (and their energies) and a two-body interaction. The problem of reference energy is briefly described in Sect. 4.2.2 and the choice of s.p. orbits, SPE and two-body interaction is given in Sect. 4.2.3. All the calculations are carried out using surface delta interaction (SDI) with one strength parameter G. The theoretical calculations involve evaluating the spreading variances and the moments for constructing NIP densities as described in Sect. 3.1. For these two, it is necessary to group the spherical orbits into unitary orbits and the choice of

unitary orbits for the above two calculations need not be the same. In general the later should be finer than the former. The unitary configurations in the former case define the classes [1] as described in [Fr-94] and using the classes and (3.4 - 3.6), the state and spin-cutoff densities are constructed. The choice of unitary orbits and the corresponding classes are given in Sect. 4.2.4. In Sect. 4.2.5, the empirical fact that in general spin-cutoff variances $\sigma^2_{\mathrm{V};J^2_z}$ are smaller compared to state density variances σ^2_{V} by $\sim 10\%$ is verified for the eight fp-shell nuclei. This result is used in the calculation of level densities in order to reduce computer time. The calculational procedure is outlined in Sect. 4.2.6. The results of the calculation of the level densities and spin-cutoff factors and their comparison with the experimental data are given in Sect. 4.3 for the six nuclei ^{55}Mn, ^{56}Fe, ^{59}Co, ^{60}Co, ^{60}Ni, ^{62}Ni and ^{63}Cu employing the space spanned over the eight spherical orbits ($1d_{5/2}$, $2s_{1/2}$, $1d_{3/2}$, $1f_{7/2}$, $2p_{3/2}$, $1f_{5/2}$, $2p_{1/2}$, $1g_{9/2}$) and in Sect. 4.4 for the nuclei ^{62}Ni, ^{63}Cu and ^{65}Cu employing the space spanned over the ten spherical orbits ($1d_{5/2}$, $2s_{1/2}$, $1d_{3/2}$, $1f_{7/2}$, $2p_{3/2}$, $1f_{5/2}$, $2p_{1/2}$, $1g_{9/2}$, $1g_{7/2}$, $2d_{5/2}$). Using ^{63}Cu nucleus as an example, it is clearly demonstrated in Sect. 4.3 that for $A > 60$ nuclei it is essential to go beyond the eight orbit space and therefore in the calculations presented in Sect. 4.4, the space of ten spherical orbits is employed. Finally a summary is given in Sect. 4.5. The results given in this chapter are first reported in [Ko-94c].

[1] Classes are defined by the unitary configurations in (3.4 - 3.6). These unitary configurations are generated by the largest possible unitary orbits (orbits α in Fig. 3.1) consistent with the definition of the S - quantum number. In fact it is the fluctuation in the spreading widths of spherical configurations that belong to a given class is small but not for the configurations that belong to a given S. It should be noted that the class variances involve partial variances unlike the fixed-S variances. Classes are introduced in [Fr-94] as they appear to provide a basis for the constant width approximation in terms of an ensemble representation of the hamiltonian.

4.2 Selection of nuclei, choice of orbits and the hamiltonian and the procedure for calculations

4.2.1 Choice of fp-shell nuclei

The experimental data for level densities and spin-cutoff factors come from four different sources and they are : (1) direct counting of levels; (2) neutron/proton resonance experiments; (3) charged particle spectra; (4) Ericson fluctuation measurements. Details of these methods are given in Appendix C. The first method gives level densities at few (2 or 3) low-lying energies (say $E \sim 2 - 4\,MeV$), the second method gives the level density at resonance energy (proton resonance experiments give densities at say 2 nearby energies), the third method gives values for level density parameters (a and Δ) say valid upto 20-25 MeV excitation and the fourth one gives level densities at a few (3 or 4) energies at high excitation energy (say around 20 MeV). Theoretical calculations need a reference energy (Sect. 4.2.2) and there is also a free parameter (G; see Sect. 4.2.3 and Appendix B) in the interaction. The low-energy data is used in fixing the reference energy and then the resonance data gives a value for G. The purpose here is not just to derive a value for G but also to verify whether one can extrapolate the predictions much beyond the resonance energy (i.e. beyond say 10 MeV and upto say $20 - 25\,MeV$ excitation). To verify this one needs data from sources (3) and/or (4). Thus, in the selection of the nuclei, for analysis with the theory given in Sect. 4.3.1, we impose the restriction that the nucleus under question should have level density data from {(1) and/or (2)} and {(3) and/or (4)}. With this restriction, there are only eight fp-shell nuclei, as given in Table 4.1, that can be analyzed. The

data for the eight nuclei listed in Table 4.1 are compiled in Appendix C.

Table 4.1 Sources of data for fp-shell nuclei. The sources (1) - (4) are defined in the text.

Nucleus	Sources of data
^{55}Mn	(1), (2), (4)
^{56}Fe	(1), (3), (4)
^{59}Co	(1), (2), (3)
^{60}Co	(2), (4)
^{60}Ni	(1), (2), (3), (4)
^{62}Ni	(1), (2), (3)
^{63}Cu	(1), (2), (3)
^{65}Cu	(1), (2), (3)

4.2.2 Reference energy

The calculated state density yields a smoothed spectrum via the distribution function $F(E) = \int_{-\infty}^{E} I(x)dx$. Given a sequence of levels with angular momentum J_1, J_2, J_3, ...J_r, inverting the equation $F(E) = \sum_{k=1}^{r-1}(2J_k+1)+(2J_r+1)/2$ gives the energy E_r of the r^{th} level. With $N_r = \sum_{k=1}^{r}(2J_k+1)$ denoting total number of states including and upto the r^{th} level, one has to solve the equation

$$\left[N_r - \frac{(2J_r+1)}{2}\right] = \int_{-\infty}^{\overline{E_r}} I(E)\,dE \tag{4.1}$$

to obtain the smoothed energy $\overline{E_r}$. For sequence of levels with fixed parity (say π), extension of (4.1) is straightforward by replacing $I(E)$ by $I^{\pi}(E)$, N_r by N_r^{π} and J_r by J_r^{π}. Using this method one can calculate the ground state energy and then measure all the energies with respect to this energy. Then comparison of calculated and experimental densities is immediate. However, as the fluctuations in low-energy domain are not "quantum chaotic", one should match the energy of a high lying level with the corresponding calculated energy

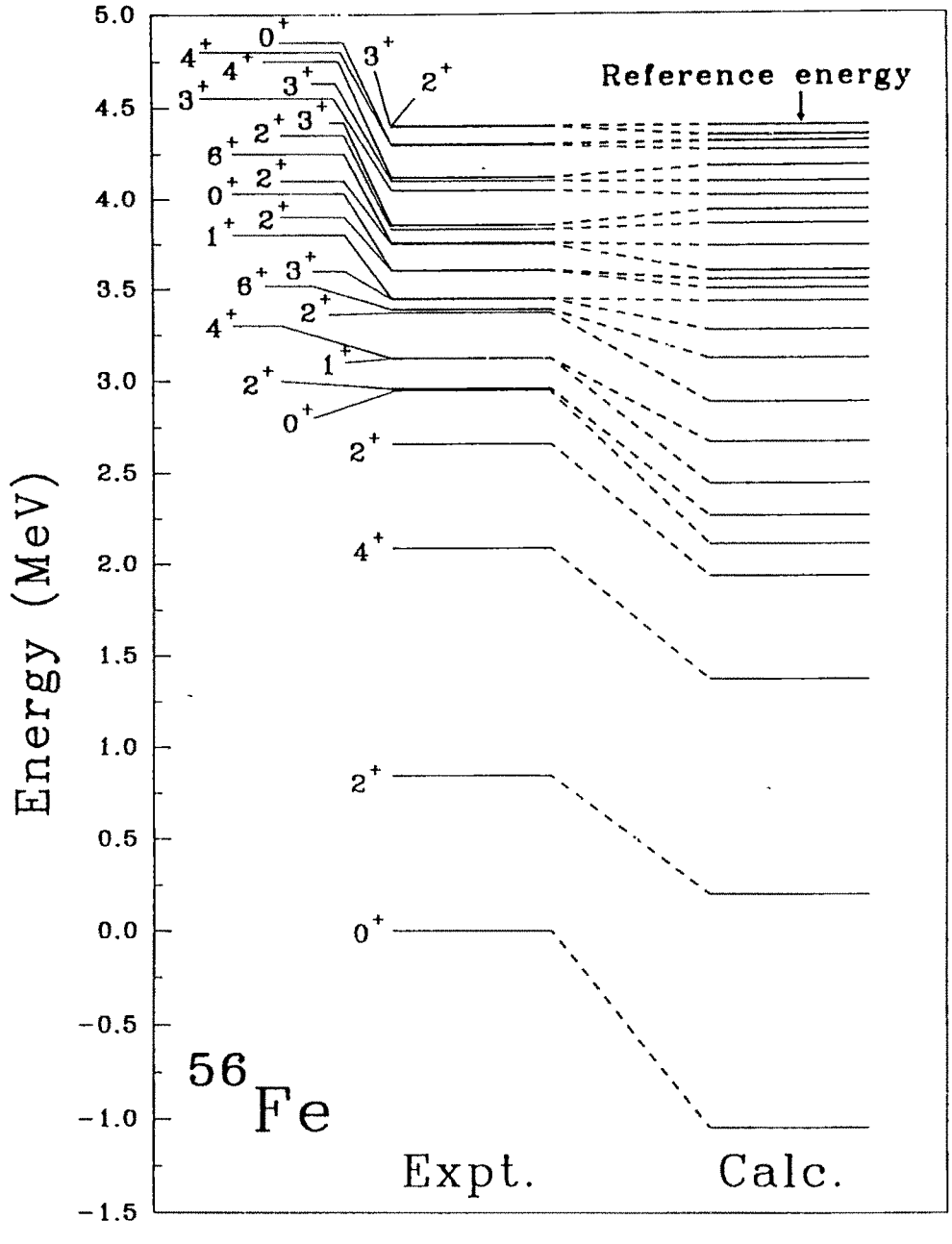

Fig. 4.1 Comparison of calculated smoothed spectrum with experimental spectrum for ^{56}Fe. Figure gives an example of reference energy selection.

as shown in Fig. 4.1 and then measure all the energies with respect to this "reference energy". There are several variants of the reference energy selection [Br-81, Fr-94]. Thus in order to proceed to the level density calculations, complete set of low-lying levels (upto a high enough energy) and the J^{π}_{ref} value of the last level (reference level) in the sequence (with energy $E_{ref}(J^{\pi}_{ref})$) are needed. This data for the eight nuclei mentioned in Table 4.1 are given in Sect. 4.3. Using $I(E) = \sum_{[\mathrm{m}]} I^{[\mathrm{m}]}(E) = \sum_{[\mathrm{m}]} d([\mathrm{m}])\rho^{[\mathrm{m}]}(E)$ as given by (3.2) with $\rho^{[\mathrm{m}]}(E)$ taken to be a Edgeworth corrected Gaussian (2.8) leads to (with N_{ref} giving the number of states upto and including the reference level),

$$\left[N_{ref} - \tfrac{1}{2}(2J_{ref}+1)\right] = \sum_{[\mathrm{m}]} d([\mathrm{m}]) \int_{-\infty}^{\overline{E}_{ref}} \rho^{[\mathrm{m}]}(E)dE \ ;$$

$$\int_{-\infty}^{\overline{E}_{ref}} \rho^{[\mathrm{m}]}(E)\, dE = \frac{1}{2} erfc\left[\frac{\epsilon([\mathrm{m}]) - \overline{E}_{ref}}{\sqrt{2}\sigma([\mathrm{m}])}\right] - \eta_{\mathcal{G}}(z)\left\{\left[\frac{k_3([\mathrm{m}])}{6} He_2(z)\right] + \left[\frac{k_4([\mathrm{m}])}{24} He_3(z) + \frac{[k_3([\mathrm{m}])]^2}{72} He_5(z)\right]\right\} \ ;$$

$$z = (\overline{E}_{ref} - \epsilon([\mathrm{m}]))/\sigma([\mathrm{m}]) \qquad (4.2)$$

Given the values of $(N_{ref},\ J^{\pi}_{ref})$ one can solve [2] (4.2) to obtain $\overline{E}_{ref}$ and match it with the experimental energy $E_{ref}(J^{\pi}_{r})$.

4.2.3 Choice of the single particle orbits and the two-body interaction

s.p. orbits and SPE

For the calculation of the level densities, eight single particle shell model orbits are chosen (for both protons and neutrons) and they are $1d_{5/2}$, $2s_{1/2}$,

[2] A simple formula for the error function is as follows [Ab-64, p. 297,299]: $erfc(z) = 1 - erf(z)$, $erfc(-z) = 1 + erf(z) = 2 - erfc(z)$; $z > 0$, $erf(x) = 1 - (a_1 t + a_2 t^2 + a_3 t^3 + a_4 t^4 + a_5 t^5)e^{-x^2} + \epsilon(x)$; $t = \frac{1}{1+px}$, $|\epsilon(x)| \leq 1.5 \times 10^{-7}$; $p = 0.3275911$, $a_1 = 0.254829592$, $a_2 = -0.284496736$, $a_3 = 1.421413741$, $a_4 = -1.453152027$, $a_5 = 1.061405429$.

$1d_{3/2}$, $1f_{7/2}$, $2p_{3/2}$, $1f_{5/2}$, $2p_{1/2}$ and $1g_{9/2}$. Thus (s^4p^{12}) is taken as the closed core and the space consists of ds - shell, fp-shell and $g_{9/2}$ orbit. The SPE given in [Sp-65] are used in the calculations and for the above eight orbits they are (in MeV) (−4.15, −3.28, 0.93, 1.55, 3.57, 7.74, 5.58, 8.74) respectively. They give the ds, fp and $g_{9/2}$ centroid energies to be −2.311, 4.214, and 8.74 MeV respectively. The $ds-fp$ and $fp-g_{9/2}$ separations then are $\Delta_{ds-fp} = 6.53\,MeV$ and $\Delta_{fp-g_{9/2}} = 4.53\,MeV$. However the interaction V produces a further renormalization of Δ_{ds-fp} and $\Delta_{fp-g_{9/2}}$ as we are considering s^4p^{12} to be a closed core; the renormalization arises (as discussed in footnote #1 of Chapter 3) due to the interaction of a particle in (ds), (fp) and $g_{9/2}$ shells with the core. The $ds - fp$ and $fp - g_{9/2}$ separations due to renormalization are calculated (given in footnote #1 of Chapter 3) using Kuo 15-orbit interaction and they are $\delta\Delta^{Kuo}_{sd-fp} = 5.66\ MeV$ and $\delta\Delta^{Kuo}_{fp-g_{9/2}} = 3.38\ MeV$. However as SDI is used for V in the present calculations, it is plausible that one need not use the above values for $\delta\Delta$. A number of level density calculations are carried out, to test the effects due to variations in $\delta\Delta$ (Sect. 4.3 gives an important

Table 4.2 Quantum numbers and energies of s.p. orbits

orbit #	s	n	ℓ	j	ϵ_j (MeV)
#1	0	0	2	5/2	-1.838
#2	0	1	0	1/2	-0.968
#3	0	0	2	3/2	3.242
#4	1	0	3	7/2	-2.664
#5	1	1	1	3/2	-0.644
#6	1	0	3	5/2	3.526
#7	1	1	1	1/2	1.366
#8	2	0	4	9/2	0.000

$\overline{\Delta}_{ds-fp} = 11.03\,MeV \quad \overline{\Delta}_{fp-g_{9/2}} = 6.53\,MeV$

discussion regarding these calculations) for all the eight fp-shell nuclei and found that it is best to use $\delta\Delta_{ds-fp} = 4.5\,MeV$ and $\delta\Delta_{fp-g_{9/2}} = 2\,MeV$. With this, the adopted (denoted by $\overline{\Delta}$) values of Δ_{ds-fp} and $\Delta_{fp-g_{9/2}}$ are $\overline{\Delta}_{ds-fp} = 11.03\,MeV$ and $\overline{\Delta}_{fp-g_{9/2}} = 6.53\,MeV$. The resulting zero centered SPE and the separations $\overline{\Delta}$, used in the calculations, are given in Table 4.2.

Two-body interaction V

The two-body interaction that has been chosen for the present calculations is the Surface Delta Interaction (SDI) with one strength parameter G as given by (B.3, B.4). Thus we have a one parameter interaction. The choice of SDI is made on the basis of its simplicity and because of the important property that SDI does not renormalize SPE (details are given in Appendix B). It is known from earlier calculations [Ko-91, Fr-94] of level densities and state densities for ^{168}Er and ^{234}U that the state density $I(E)$ (and so also the level density) varies rapidly with G. Since the value of G has to be fixed by fitting to experimental data, some knowledge of variation of $I(E)$ with G for fp-shell nuclei is essential. This variation is investigated with ^{56}Fe and ^{60}Ni as examples and the results are shown in Fig. 4.2. One sees a rapid variation in $I(E)$ with G for a given E. Thus G can be determined with precision by using level density data.

4.2.4 Unitary orbits for spreading variances and NIP calculations

For calculating state and spin-cutoff density variances, the eight spherical orbits given in Table 4.2 for protons (and neutrons) are divided into three unitary orbits (denoted by UOV). The UOV orbits and the corresponding s values are

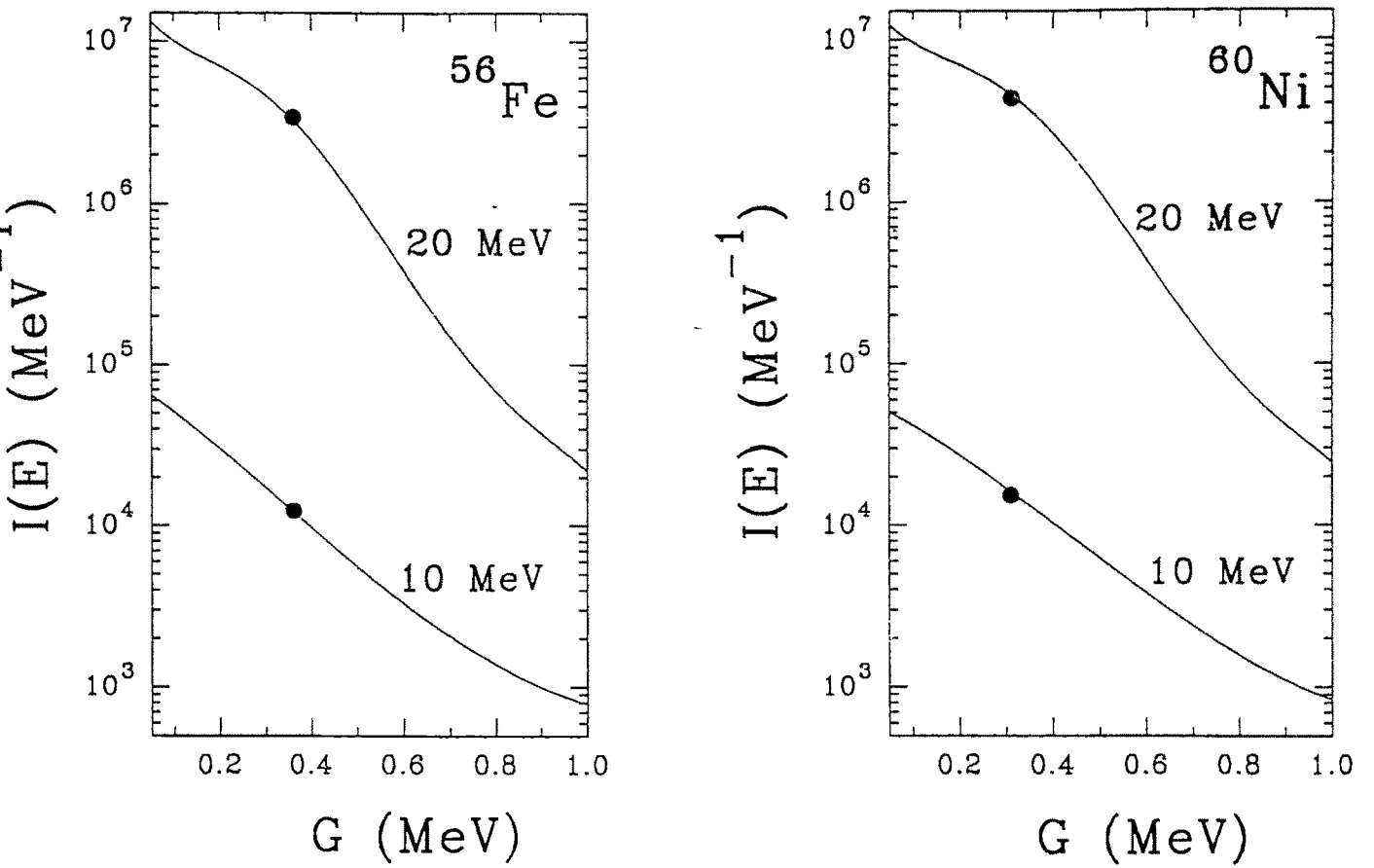

Fig. 4.2 State density $I(E)$ vs G for ^{56}Fe and ^{60}Ni at $E = 10\ MeV$ and $20\ MeV$. The value of G used in the level density calculations is shown by filled circles.

given in Table 4.3. Given a fp-shell nucleus, the proton and neutron numbers (m_p, m_n) outside the s^4p^{12} core can be easily counted. The smallest total S value allowed for the nucleus is given by $S_{min} = m_p + m_n - 24$. Given a unitary configuration $[\mathbf{m}_p, \mathbf{m}_n]$ defined over the UOV given in Table 4.3, the total S value $S_{TOT}([\mathbf{m}_p, \mathbf{m}_n]) = \sum_{i=1}^{3}(\mathbf{m}_p)_i s_i + \sum_{i=1}^{3}(\mathbf{m}_n)_i s_i$. Then the $S\hbar\omega$ excitations are given by $S = S([\mathbf{m}_p, \mathbf{m}_n]) = S_{TOT}([\mathbf{m}_p, \mathbf{m}_n]) - S_{min}$. The calculations in this chapter are restricted to $2\hbar\omega$ excitations, i.e. $S \leq 2$. As already mentioned before, the classes are defined by $[\mathbf{m}_p, \mathbf{m}_n]$. There are one $S = 0$, four $S = 1$ and ten $S = 2$ classes. The S values and the corresponding classes are given in Table 4.4. In Table 4.4 whenever Λ_{-1} is not shown, it implies that Λ_{-1} orbit is full. Similarly Λ_1 orbit is not shown whenever it is empty. For the calculation of the NIP densities $I^{\mathbf{h}}(E)$, and $I^{\mathbf{h}}_{J_Z^2}(E)$, three UOV unitary orbits are further divided into five unitary orbits (denoted by UON) as given in Table 4.5. For each nucleus, the number of unitary configurations defined by UON unitary orbits for each of the 15 classes are given in Table 4.6. From Tables 4.4 and 4.6 it is seen that for spreading variance calculations there are 11 configurations for +ve parity states and for both parities 15 configurations while for NIP calculations and in the final sum (using (3.4 - 3.6)) involving convolution of NIP and spreading Gaussian densities there are $\sim$ 1500 configurations for both parities. However, with spherical orbits for both UOV and UON orbits, there will be $\sim 10^4$ configurations and then one has to calculate $\sim 10^4$ spreading variances unlike only 15 with UOV unitary orbits.

Table 4.3 Unitary orbits (UOV) for spreading variance calculations. Given in the table are also the s values of and symbols for each unitary orbit.

UOV #	Spherical orbits	s value	symbol
#1	$d_{5/2}$, $s_{1/2}$, $d_{3/2}$	0	Λ_{-1}
#2	$f_{7/2}$, $p_{3/2}$, $f_{5/2}$, $p_{1/2}$	1	Λ_0
#3	$g_{9/2}$	2	Λ_1

Table 4.4 Class structures. Table 4.3 defines the symbol Λ_i.

S	Class Structure	Class No.
0	$(\Lambda_0)^{m_p}(\Lambda_0)^{m_n}$	#1
1	$(\Lambda_0)^{m_p}(\Lambda_{-1})^{m_n-1}(\Lambda_1)^{1_n}$	#2
	$(\Lambda_0)^{m_p}(\Lambda_{-1})^{-1_n}(\Lambda_0)^{m_n+1}$	#3
	$(\Lambda_{-1})^{m_p-1}(\Lambda_1)^{1_p}(\Lambda_0)^{m_n}$	#4
	$(\Lambda_{-1})^{-1_p}(\Lambda_0)^{m_p+1}(\Lambda_0)^{m_n}$	#5
2	$(\Lambda_0)^{m_p}(\Lambda_0)^{m_n-2}(\Lambda_1)^{2_n}$	#6
	$(\Lambda_0)^{m_p}(\Lambda_{-1})^{-1_n}(\Lambda_0)^{m_n}(\Lambda_1)^{1_n}$	#7
	$(\Lambda_0)^{m_p}(\Lambda_{-1})^{-2_n}(\Lambda_0)^{m_n+2}$	#8
	$(\Lambda_0)^{m_p-1}(\Lambda_1)^{1_p}(\Lambda_0)^{m_n-1}(\Lambda_1)^{1_n}$	#9
	$(\Lambda_0)^{m_p-1}(\Lambda_1)^{1_p}(\Lambda_{-1})^{-1_n}(\Lambda_0)^{m_n+1}$	#10
	$(\Lambda_0)^{m_p-2}(\Lambda_1)^{2_p}(\Lambda_0)^{m_n}$	#11
	$(\Lambda_{-1})^{-1_p}(\Lambda_0)^{m_p+1}(\Lambda_0)^{m_n-1}(\Lambda_1)^{1_n}$	#12
	$(\Lambda_{-1})^{-1_p}(\Lambda_0)^{m_p+1}(\Lambda_{-1})^{-1_n}(\Lambda_0)^{m_n+1}$	#13
	$(\Lambda_{-1})^{-1_p}(\Lambda_0)^{m_p}(\Lambda_1)^{1_p}(\Lambda_0)^{m_n}$	#14
	$(\Lambda_{-1})^{-2_p}(\Lambda_0)^{m_p+2}(\Lambda_0)^{m_n}$	#15

Table 4.5 Unitary orbits (UON) for NIP calculations. Given also are the s - values for each unitary orbit.

UON #	Spherical orbits	s
#1	$d_{5/2}, s_{1/2}$	0
#2	$d_{3/2}$	0
#3	$f_{7/2}$	1
#4	$p_{3/2}, f_{5/2}, p_{1/2}$	1
#5	$g_{9/2}$	2

Table 4.6 Number of unitary configuration for NIP calculations

Class #	Nucleus							
	^{55}Mn	^{56}Fe	^{59}Co	^{60}Co	^{60}Ni	^{62}Ni	^{63}Cu	^{65}Cu
#1	54	63	72	64	81	63	63	45
#2	54	63	72	72	81	72	72	54
#3	108	126	128	112	144	108	108	72
#4	45	54	63	56	72	63	56	45
#5	126	144	162	144	162	126	126	90
#6	54	63	72	72	81	81	81	63
#7	108	126	144	128	162	126	126	90
#8	162	189	168	144	189	135	135	81
#9	45	54	63	63	72	64	72	54
#10	90	108	112	98	128	96	108	72
#11	36	45	54	48	63	49	56	40
#12	126	144	162	162	162	144	144	108
#13	252	288	288	252	288	216	216	144
#14	108	126	144	128	162	126	126	90
#15	216	243	243	216	243	189	189	135

4.2.5 Ratio of J^2-density variance and state density variance

From the previous level density calculations for ^{28}Si, ^{168}Er, ^{181}W and ^{234}U nuclei [Ko-91, Ko-93a, Fr-94] it is found that in general the J^2-density variance is smaller, $\sim$30% of the state density variance for all class members. Using this result will considerably reduce the computing time. On the machine

that is available to us it takes $\sim$ 80 hours for calculating $\sigma^2_{\mathbf{V};J^2_z}$ for all the 15 classes listed in Table 4.4 against $\sim$ 4 minutes for calculating the spreading variances $\sigma^2_{\mathbf{V}}$ for the 15 classes. Thus the 8 - orbit calculations are impractical but however calculations are easy to carry out if the result $\sigma^2_{\mathbf{V};J^2_z}/\sigma^2_{\mathbf{V}} \sim 0.9$ is used. Before using this result in the present calculations, it should be verified for fp-shell nuclei. In order to do this, we have chosen a 7-orbit space consisting of ($2s_{1/2}$, $1d_{3/2}$, $1f_{7/2}$, $2p_{3/2}$, $1f_{5/2}$, $2p_{1/2}$, $1g_{9/2}$) spherical orbits and the corresponding unitary orbit numbers are (#1, #1, #2, #2, #2, #2, #3) respectively. Thus in the 7-orbit calculations Λ_{-1} of Table 4.3 contains only $2s_{1/2}$ and $1d_{3/2}$ orbits. It should be clear that there is a one to one correspondence between the 7-orbit and 8-orbit classes. For each of the 15 classes given in the Table 4.4 the ratio $\sigma^2_{\mathbf{V}}/\sigma^2_{\mathbf{V};J^2_z}$ is observed to be $\sim$ 1.09 and the results are given in Table 4.7; the 7-orbit calculations for each nucleus

Table 4.7 The ratio $\sigma^2_{\mathbf{V}}/\sigma^2_{\mathbf{V};J^2_z}$ for fp-shell nuclei in a 7-orbit calculation

Class #	$\sigma^2_{\mathbf{V}}/\sigma^2_{\mathbf{V};J^2_z}$							
	^{55}Mn	^{56}Fe	^{59}Co	^{60}Co	^{60}Ni	^{62}Ni	^{63}Cu	^{65}Cu
#1	1.11	1.11	1.10	1.11	1.10	1.11	1.11	1.11
#2	1.09	1.08	1.08	1.08	1.08	1.08	1.08	1.08
#3	1.09	1.09	1.08	1.09	1.08	1.08	1.08	1.08
#4	1.09	1.08	1.08	1.08	1.08	1.08	1.08	1.08
#5	1.09	1.09	1.09	1.09	1.09	1.09	1.09	1.09
#6	1.08	1.07	1.07	1.07	1.07	1.07	1.07	1.07
#7	1.07	1.07	1.07	1.07	1.07	1.07	1.07	1.07
#8	1.07	1.07	1.07	1.07	1.07	1.07	1.07	1.07
#9	1.07	1.07	1.07	1.07	1.07	1.07	1.07	1.07
#10	1.07	1.07	1.07	1.07	1.07	1.07	1.07	1.07
#11	1.08	1.08	1.07	1.07	1.07	1.07	1.07	1.07
#12	1.08	1.07	1.07	1.07	1.07	1.07	1.07	1.07
#13	1.08	1.08	1.08	1.08	1.08	1.08	1.07	1.07
#14	1.08	1.08	1.07	1.07	1.07	1.07	1.07	1.07
#15	1.08	1.08	1.08	1.08	1.08	1.08	1.08	1.08

takes $\sim$ 4 hours of computing time. In ^{56}Fe example full 8-orbit calculations for $\sigma^2_{\mathbf{V}:J^2_Z}$ are carried out for all the 15 classes given in Table 4.4. The 8-orbit $\sigma^2_{\mathbf{V}}/\sigma^2_{\mathbf{V}:J^2_Z}$ values for each of the 15 classes are found to be essentially identical (within 1%) to the 7-orbit numbers given in Table 4.7. This result permits us to use the results of Table 4.7 in 8-orbit calculations.

The results discussed above are employed in calculating the spreading variances as follows. Using propagation methods given in Sect. 2.6 the state density spreading variances $\sigma^2_{\mathbf{V}}$ are calculated for each of the 15 classes in 8-orbit case. Using the 8-orbit values for $\sigma^2_{\mathbf{V}}$ and the 7-orbit results (from Table 4.7) for $\sigma^2_{\mathbf{V}}/\sigma^2_{\mathbf{V}:J^2_Z}$, $\{\sigma^2_{\mathbf{V}:J^2_Z}\}_{8-orbit}$ is computed using $\sigma^2_{\mathbf{V}:J^2_Z} = \{\sigma^2_{\mathbf{V}}\}_{8-orbit} \times \left[\{\sigma^2_{\mathbf{V}}/\sigma^2_{\mathbf{V}:J^2_Z}\}_{7-orbit}\right]^{-1}$. These effective 8-orbit $\sigma^2_{\mathbf{V}:J^2_Z}$ values together with centroid shifts $\epsilon_{\mathbf{V}:J^2_Z}$ are used in constructing the spin-cutoff densities.

4.2.6 Procedure for calculations

Following the theory outlined in Sect. 3.1, for calculating level densities and spin-cutoff factors, first the unitary decomposition (with respect to the direct sum group defined by UOV orbits) of the hamiltonian ($h + V$; h defined by SPE in Table 4.2 and $V = G \times (SDI)$) and J^2 operator are carried out. Then, for each of the fifteen classes given in Table 4.4, the spreading variances $\sigma^2_{\mathbf{V}}([\mathbf{m}])$ and centroid shifts $\epsilon_{\mathbf{V}:J^2_Z}([\mathbf{m}])$ are obtained. Using the method described in Sect. 4.2.5 the spin-cutoff density variances $\sigma^2_{\mathbf{V}:J^2_Z}([\mathbf{m}])$ are calculated. Generating the configurations $\{\mathbf{m}\}$ defined by UON orbits for each of the 15 classes (defined by UOV orbits), the first four NIP density cumulants $\epsilon_{NIP}(\{\mathbf{m}\})$, $\sigma^2_{NIP}(\{\mathbf{m}\})$, $\gamma_1^{NIP}(\{\mathbf{m}\})$ and $\gamma_2^{NIP}(\{\mathbf{m}\})$ are calculated (the number of $\{\mathbf{m}\}$ in a $[\mathbf{m}]$ is given in Table 4.6) both for NIP state and spin-cutoff

densities. The $I^h \otimes \rho^V$ convolution, for each $\{\mathbf{m}\} \in [\mathbf{m}]$, is carried out by adding the I^h and ρ^V cumulants (in the present exercise ρ^V is a Gaussian). Using the first four cumulants (ϵ, σ^2, γ_1, γ_2) thus obtained, the fixed $\{\mathbf{m}\}$ densities are written as Edgeworth corrected Gaussian densities (2.8). The above exercise is carried out for positive parity configurations in case of even-even or odd-odd nuclei and for negative parity configurations in case of even-odd or odd-even nuclei in our set. All the calculations use $S = 0 \oplus S = 2$ space. The ratio of these fixed-parity spin-cutoff and state densities give the fixed parity spin-cutoff factors. This information is then converted into total level densities and spin-cutoff factors by using (C.8, C.12, C.13).

In the actual calculations, starting with the reference energy data (E_{ref}, J^{π}_{ref}, N_{ref}) given ahead in Sect. 4.3 and a value for the SDI strength G ($G \simeq 25/A$ MeV), $N^{\pi}(E)$ is calculated at various energies E and then (4.2) is used to obtain $\overline{E}_{ref}$. Then the ground state energy in the calculation is $E_{GS} = \overline{E}_{ref} - E_{ref}$. Now $I^{\pi}(E)$ is calculated at around 10 MeV excitation where resonance or some other data for $I_{\ell}(E)$ is available (we call it $I_{\ell;href}(E)$). The $I^{\pi}(E)$ is converted into $I_{\ell}(E)$ and compared with $I_{\ell;href}(E)$. The value of G is varied until the calculated $I_{\ell}(E)$ is within say 5% of the $I_{\ell;href}(E)$. Using the G-value thus obtained, $I_{\ell}(E)$, $I(E)$ and $\sigma_J(E)$ are calculated for E from 4 to 25 MeV excitation and compared with data.

Good agreements with data alone do not justify that the calculations are proper. It is essential that (i) in the low-energy domain (say $E \lesssim 6\,MeV$) the $S = 0$ densities should be much larger than the $S = 2$ densities ($I(E) = I_{S=0}(E) + I_{S=2}(E)$) and (ii) the value of G should be in a meaningful domain (low-energy spectroscopic calculations yield $G \simeq 25/A$ MeV). In fact the

Δ_{ds-fp} and $\Delta_{fp-g_{9/2}}$ separations (one set for all nuclei) given in Sect 4.2.3 are chosen such that for all the fp-shell nuclei under consideration the condition (i) above is satisfied and to get good agreement with data $G \simeq 20/A\ MeV$ is used. Table 4.8 shows the S-decomposititon of the state densities at various

Table 4.8 S-decomposition of state densities. For a given nucleus and a given energy, the first entry is for $I^{\pi}_{\ell;S=0}(E)$ and the second for $I^{\pi}_{\ell;S=2}(E)$. The parity $\pi = +$ for even-even nuclei and $\pi = -$ for even-odd or odd-even nuclei respectively. In Sect. 4.3.6 ahead $^{63}Cu(a)$ and $^{63}Cu(b)$ calculations are defined.

E (MeV)	^{55}Mn	^{56}Fe	^{59}Co	^{60}Co	^{60}Ni	$^{63}Cu\ (a)$	$^{63}Cu\ (b)$
4.0	24	9	26	258	14	26	6
	7	2	4	47	1	6	25
8.0	338	140	350	2608	216	333	93
	144	42	97	988	23	136	513
12.0	3100	1479	3244	18546	2256	3002	1021
	2109	692	1613	14322	511	2304	7379
16.0	20121	11171	22046	97501	17057	19813	7934
	23607	8694	19914	150780	8015	28196	78174
20.0	96461	27442	113900	393590	97154	99534	45869
	204080	28022	187940	1201100	92063	260010	631190

energies for the six nuclei $\{^{55}Mn, ^{56}Fe, ^{59}Co, ^{60}Co, ^{60}Ni, ^{63}Cu\}$. In the case of ^{63}Cu using densities corresponding to $^{63}Cu\ (b)$ in Table 4.8, one gets excellent agreement with data as described in Sect. 4.3.6 ahead. However here the $S = 2$ densities are much larger than $S = 0$ densities. Thus these calculations cannot be considered to be good (similar problems exist in the preliminary calculations for ^{56}Fe reported in [Ja-92]). However this is not the case with the $^{63}Cu\ (a)$ calculations though here the agreements are only satisfactory as shown in Fig. 4.10 ahead.

4.3 8-orbit results for ^{55}Mn, ^{56}Fe, ^{59}Co, ^{60}Co, ^{60}Ni and ^{63}Cu

Following Sect. 4.2, level densities and spin-cutoff factors are calculated for the eight nuclei $\{^{55}Mn, ^{56}Fe, ^{59}Co, ^{60}Co, ^{60}Ni, ^{62}Ni, ^{63}Cu, ^{65}Cu\}$. It is found that $A > 60$ nuclei, the space defined by the eight orbits $\{1d_{5/2}, 2s_{1/2}, 1d_{3/2}, 1f_{7/2}, 2p_{3/2}, 1f_{5/2}, 2p_{1/2}, 1g_{9/2}\}$ is not adequate. For the three nuclei ^{62}Ni, ^{63}Cu and ^{65}Cu, the calculated densities differ from data values by a factor 2-3 and it is clearly seen that in these cases to get good agreements one has to necessarily violate the conditions (i) and (ii) given in Sect. 4.2.6. The problems encountered here are discussed in some detail with the ^{63}Cu example in Sect 4.3.6. Because of the problem mentioned above, detailed calculations are carried out only for the six nuclei $\{^{55}Mn, ^{56}Fe, ^{59}Co, ^{60}Co, ^{60}Ni, ^{63}Cu\}$ and compared with data in Sects. 4.3.1 – 4.3.6. It appears that the solution to the problems encountered with $A > 60$ nuclei can be solved only by expanding the space, i.e. by including $(2d_{5/2}, 1g_{7/2})$ orbits or in other words by performing 10-orbit calculations for these nuclei. This aspect is discussed in Sect. 4.3.6 and the results of 10-orbit calculations are given in Sect. 4.4. All the calculations reported in Sects. 4.3.1 – 4.3.6 and 4.4 are performed using the package LVLDN_INT [Ha-92].

4.3.1 Nucleus ^{55}Mn

The low-energy data which is used in fixing the reference energy are given in Table 4.9. Also shown in the table are E_{ref}, J^{π}_{ref} and N_{ref} values and with these values,

Table 4.9 Low energy data for reference energy calculation

E (MeV)	J^π	Ref
0.0	$5/2^-$	[Nu-85]
0.126	$7/2^-$	[Nu-85]
0.984	$9/2^-$	[Nu-85]
1.290	$1/2^-$	[Le-78]
1.292	$11/2^-$	[Nu-85]
1.293	$1/2^-$	[Nu-85]
1.528	$3/2^-$	[Nu-85]
$E_{ref} = 1.528\ MeV$		$J^\pi_{ref} = 3/2^-$
	$N_{ref} = 44$	

the GS energy is calculated, with a trial value of G, using the method outlined in Sect. 4.2.2. The value of G is varied such that the total level density $I_\ell(E)$ at $E = 10\ MeV$ becomes close to the values obtained from the experimental (proton resonance) data compiled by Iljinov et al (Table C.1) which is $3000 \pm 800\, MeV^{-1}$. With $G = 0.365\, MeV$ the calculated value of $I_\ell(E)$ at $10\ MeV$ is 3200 MeV^{-1}. The values of $\sigma^2_{\mathbf{V}}$, $\sigma^2_{\mathbf{V};J^2_z}$ and $\epsilon_{\mathbf{V};J^2_z}$ calculated with $G = 0.365\, MeV$ are 17.2 MeV^2, 15.5 MeV^2 and 0.015 MeV respectively for $S = 0$ configuration, $\sim 25\ MeV^2$, $\sim 23\ MeV^2$ and $\sim 0.01\ MeV$ respectively for $S = 1$ configurations, $\sim 33\ MeV^2$, $\sim 30\ MeV^2$ and $\sim 0.02\ MeV$ respectively for $S = 2$ configurations. With the class variances and centroid shifts, $I(E)$, $I_\ell(E)$ and $\sigma_J(E)$ are calculated at various energies using the procedures given in Sect. 4.2.6 and the results are compared with data in Figs. 4.3, 4.4. From Fig. 4.3, it is seen that the agreement between data and calculations is good upto $\sim 16\, MeV$ and the departures appear to be significant beyond say 22 MeV. The calculated spin-cutoff factors are in excellent agreement with Katsanos et al data (Table C.2). The calculated state densities are fitted to the Lang LeCouteur (LLC) and back shifted Fermi gas forms (C.1, C.3, C.4) and the parameters (a, Δ) obtained from best fit are given in Table 4.10.

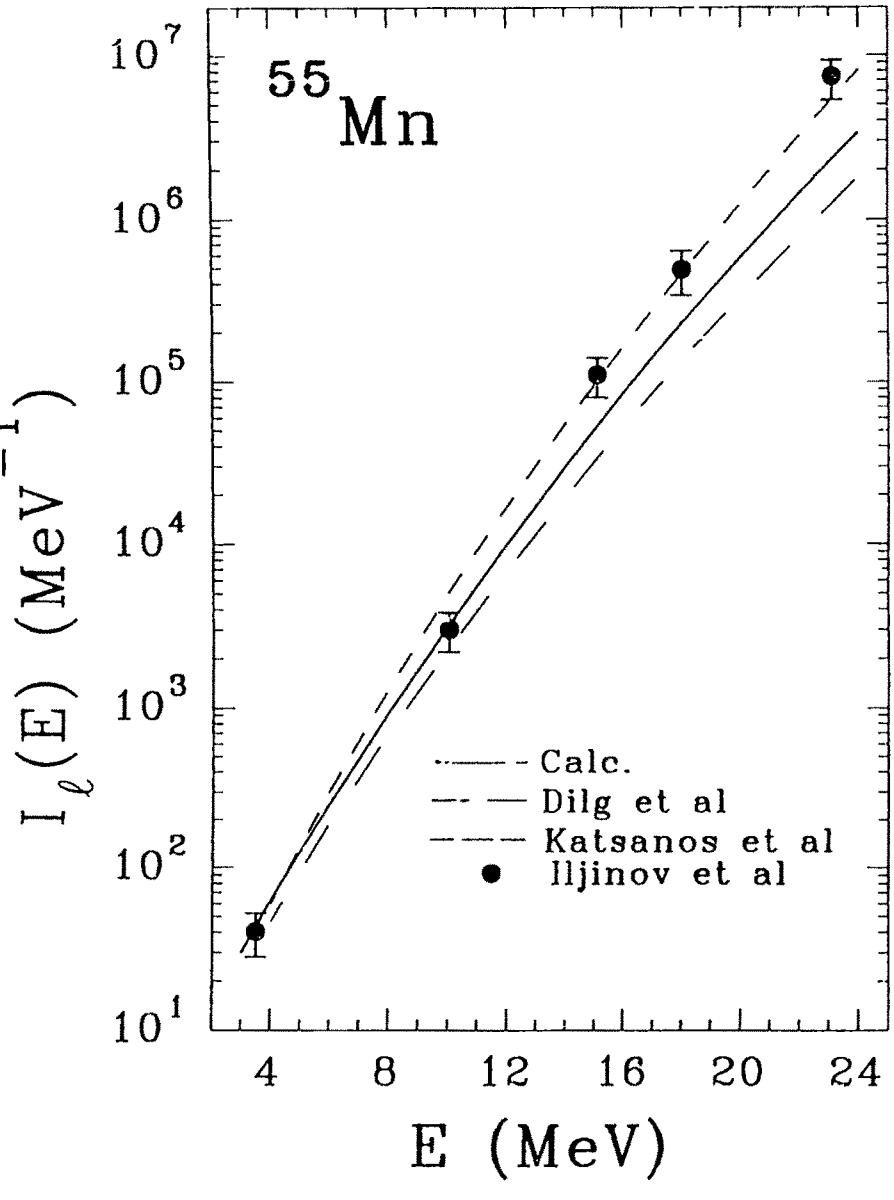

Fig. 4.3 Total level density $I_\ell(E)$ vs E for ^{55}Mn. References to data (Dilg et al, Katsanos et al, Iljinov et al) and the actual data values are given in Appendix C.

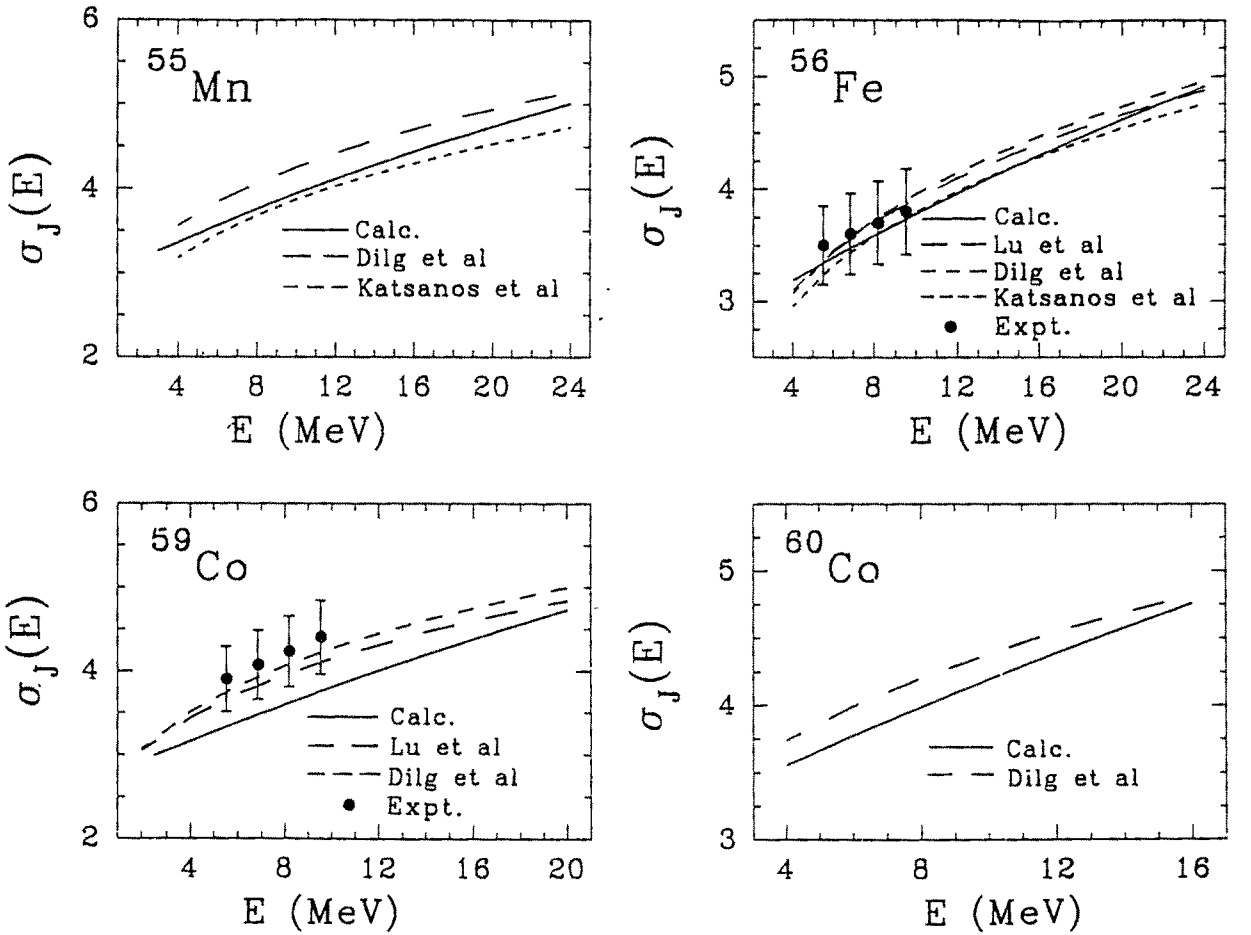

Fig. 4.4 Square root of spin-cutoff factor $\sigma_J(E)$ vs E for ^{55}Mn, ^{56}Fe, ^{59}Co, ^{60}Co, ^{60}Ni, ^{62}Ni, ^{63}Cu, ^{65}Cu. References to experimental data, data due to Dilg et al. Katsanos et al and Lu et al and actual data values are given in Appendix C.

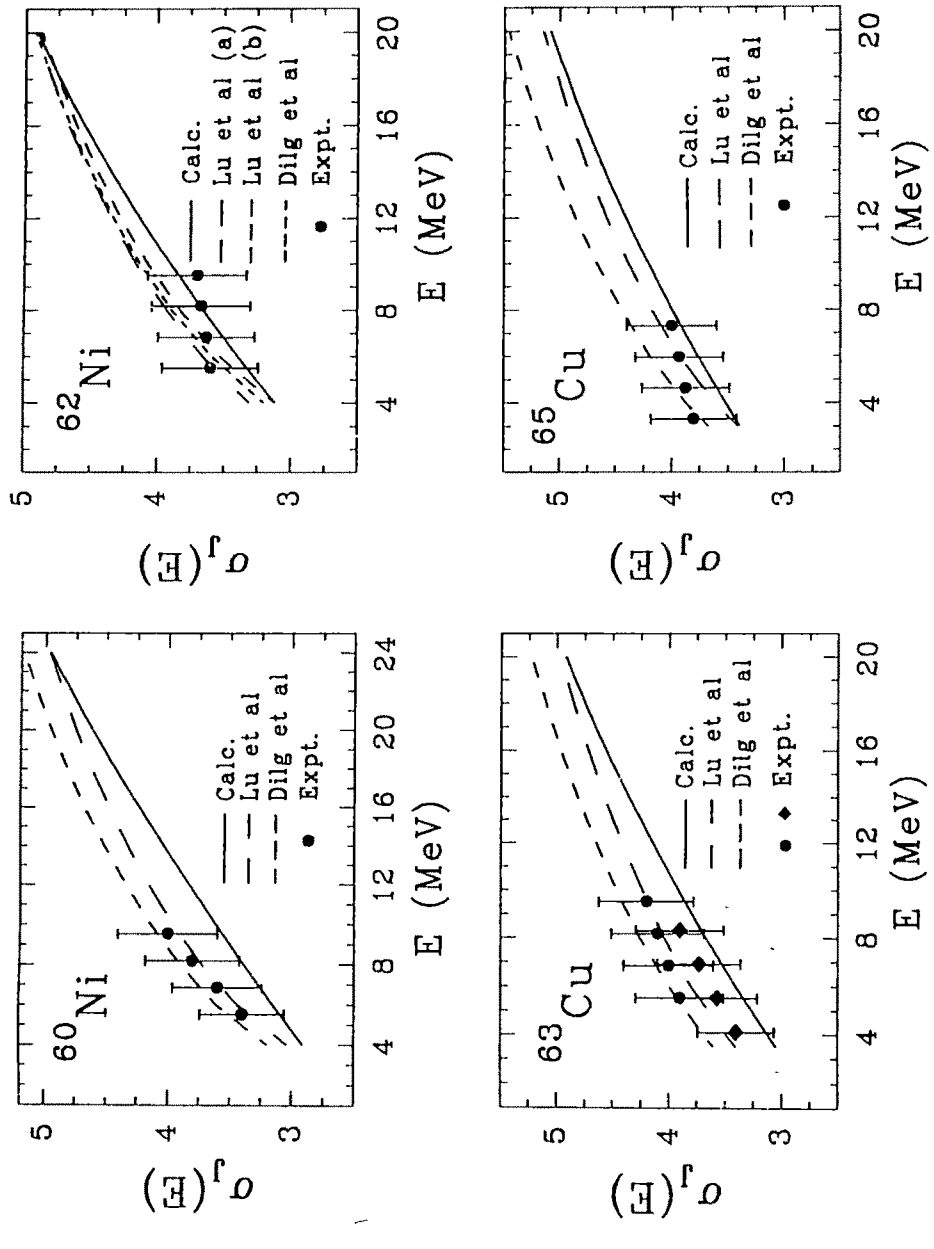
^{62}Ni
^{65}Cu
^{60}Ni
^{63}Cu
Calc.
Lu et al (a)
Lu et al (b)
Lu et al
Dilg et al
Expt.
$\sigma_J(E)$
E (MeV)

Fig. 4.4 (cont'd)

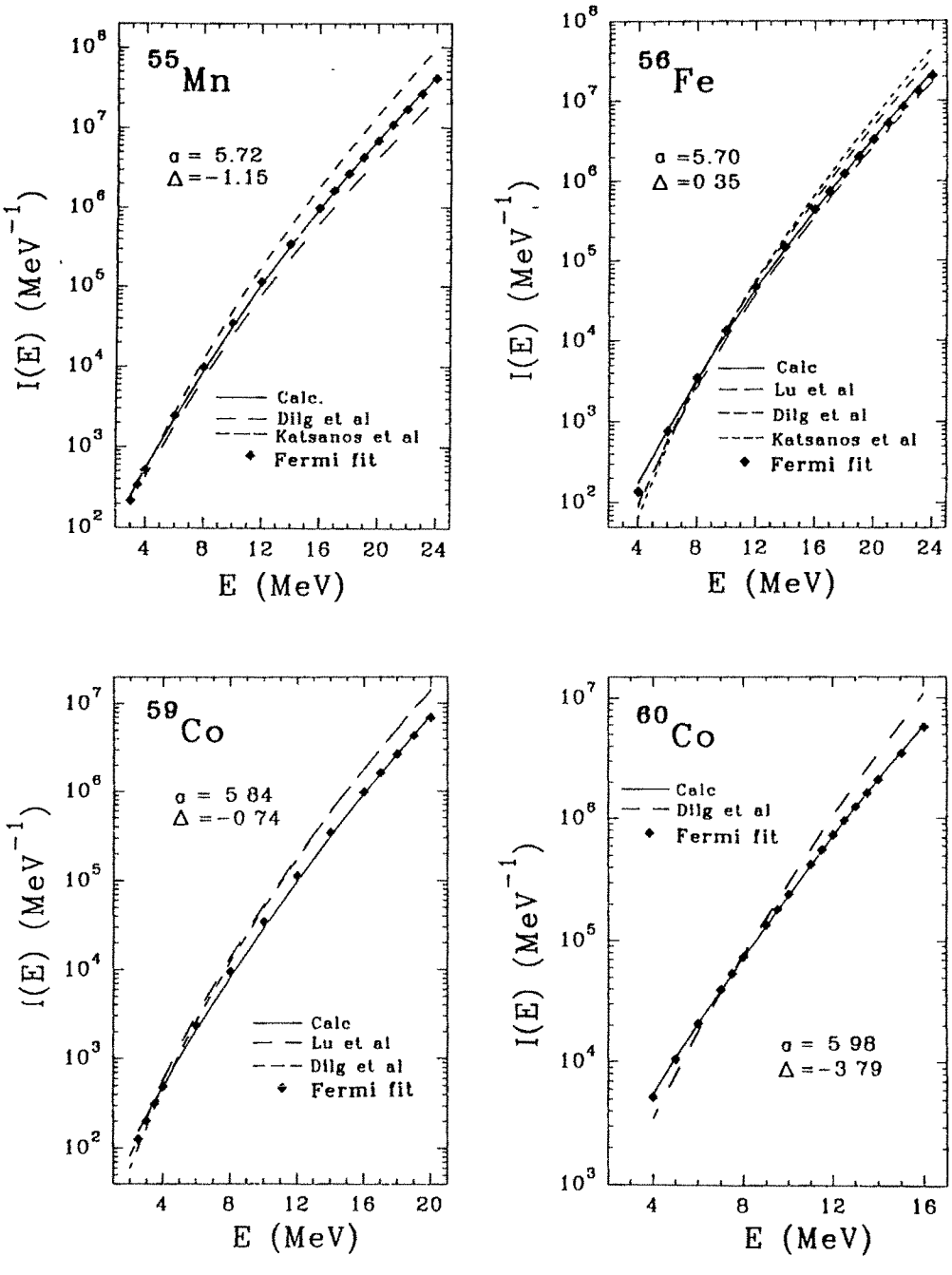

Fig. 4.5 State density $I(E)$ vs E. Filled diamonds in the figure correspond to Fermi gas fit to the calculated state density; as described in the text, the Lang LeCouteur Fermi gas formula is used in the fits. The calculated $I(E)$ is also compared with Dilg et al, Katsanos et al and Lu et al data. The Dilg et al, Katsanos et al and Lu et al data are tabulated in Appendix C.

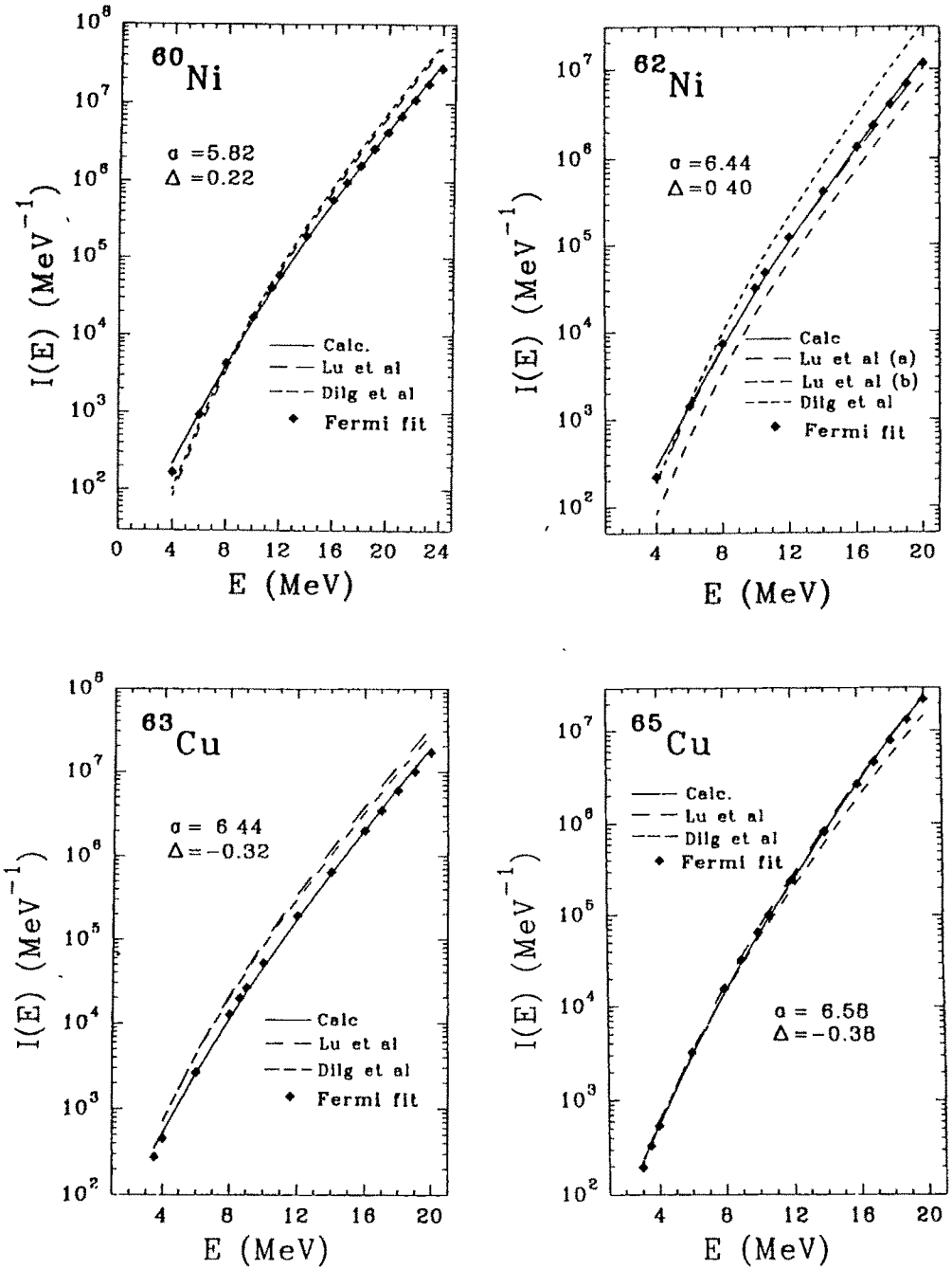
60Ni
a =5.82
Δ =0.22
Calc.
Lu et al
Dilg et al
Fermi fit
I(E) (MeV-1)
E (MeV)
62Ni
a =6.44
Δ =0 40
Calc
Lu et al (a)
Lu et al (b)
Dilg et al
Fermi fit
I(E) (MeV-1)
E (MeV)
63Cu
a = 6 44
Δ =−0.32
Calc
Lu et al
Dilg et al
Fermi fit
I(E) (MeV-1)
E (MeV)
65Cu
Calc.
Lu et al
Dilg et al
Fermi fit
a = 6.58
Δ =−0.38
I(E) (MeV-1)
E (MeV)

Fig. 4.5 (cont'd)

Table 4.10 Fermi gas parameters

Nucleus	Dilg et al		Katsanos et al		Present Calculation	
	a (MeV^{-1})	Δ (MeV)	a (MeV^{-1})	Δ (MeV)	a (MeV^{-1})	Δ (MeV)
^{55}Mn	5.45	1.20	6.30	-0.50	5.52*	-1.15*
					5.74@	-0.85@

* for Lang LeCouteur Fermi gas form @ for back shifted Fermi gas form

As can be seen from Fig. 4.5 the calculated densities are well represented by the LLC Fermi gas form. Only the LLC Fermi gas fit is shown in the figure as we are comparing our results with Dilg et al and Katsanos et al (a, Δ) values and these authors deduced (a, Δ) values using LLC form. As can be seen from Table 4.10 the deduced (a, Δ) values are compatible more with Dilg et al values than the Katsanos et al values.

4.3.2 Nucleus ^{56}Fe

The low-energy data which is used in fixing the reference energy are given in Table 4.11. Also shown in the table are E_{ref}, J^{π}_{ref} and N_{ref} values and with these values, the GS energy is calculated with a trial value of G using the method outlined in Sect. 4.2.2. The value of G is obtained such that it fits reasonably well with (there is no resonance data for ^{56}Fe) the Dilg et al (1385 MeV^{-1}), Lu et al (1064 MeV^{-1}) and Katsanos et al (1476 MeV^{-1}) data for $I_\ell(E)$ at 10 MeV excitation. At this energy the calculated $I_\ell(E) = 1304\,MeV^{-1}$ for $G = 0.36\,MeV$. For example, $\sigma^2_{\mathbf{V}}$, $\sigma^2_{\mathbf{V};J^2_Z}$ and $\epsilon_{\mathbf{V};J^2_Z}$ calculated with $G = 0.36\,MeV$ are 18.7 MeV^2, 16.9 MeV^2 and 0.006 MeV respectively for $S = 0$ configuration, $\sim$ 25 MeV^2, $\sim$ 23 MeV^2 and $\sim$ 0.01 MeV respectively for $S = 1$ configurations and $\sim$ 34 MeV^2, $\sim$ 32 MeV^2

Table 4.11 Low energy data for reference energy calculation

E (MeV)	J^π	Ref	E (MeV)	J^π	Ref
0.0	0^+	[Le-78]	3.607	0^+	[Le-78]
0.847	2^+	[Le-78]	3.748	2^+	[Nu-77]
2.085	4^+	[Le-78]	3.756	6^+	[Le-78]
2.658	2^+	[Le-78]	3.832	2^+	[Le-78]
2.942	0^+	[Le-78]	3.857	3^+	[Le-78]
2.960	2^+	[Le-78]	4.049	3^+	[Nu-77]
3.120	1^+	[Le-78]	4.100	3^+	[Nu-77]
3.123	4^+	[Le-78]	4.120	4^+	[Le-78]
3.372	2^+	[Le-78]	4.293	4^+	[Nu-77]
3.388	6^+	[Le-78]	4.302	0^+	[Nu-77]
3.445	3^+	[Le-78]	4.395	3^+	[Le-78]
3.449	1^+	[Le-78]	4.401	2^+	[Nu-77]
3.602	2^+	[Le-78]			

$E_{ref} = 4.401\ MeV$ $\qquad$ $J^\pi_{ref} = 2^+$

$N_{ref} = 147$

Table 4.12 Fermi gas parameters

Nucleus	Lu et al		Dilg et al		Katsanos et al		Present Calculation	
	a (MeV^{-1})	Δ (MeV)	a (MeV^{-1})	Δ (MeV)	a (MeV^{-1})	Δ (MeV)	a (MeV^{-1})	Δ (MeV)
^{56}Fe	5.70	0.70	6.15	1.10	6.40	1.50	5.7* 5.72@	0.35* 0.64@

* for Lang LeCouteur Fermi gas form @ for back shifted Fermi gas form

and $\sim 0.02\ MeV$ respectively for $S = 2$ configurations. With these variances and centroid shifts $I(E)$, $I_\ell(E)$ and $\sigma_J(E)$ are calculated upto 24 MeV, using the procedure outlined in Sect. 4.2.6 and the results are compared with data in Figs. 4.6, 4.4. Fig. 4.6 shows that the calculations are in excellent agreement with data right upto 24 MeV. The low-lying data (upto 6 MeV) from direct

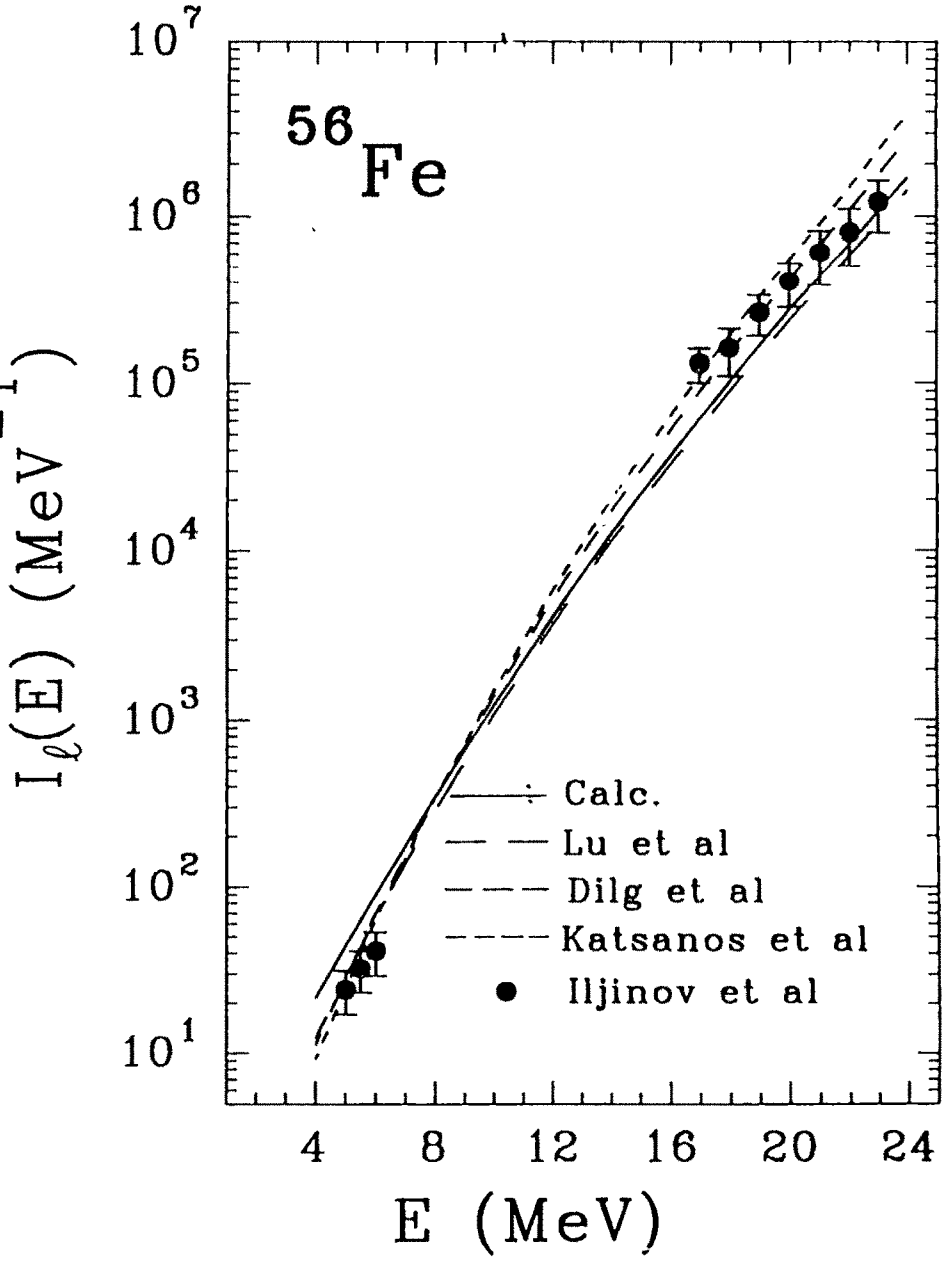

Fig. 4.6 Total level density $I_\ell(E)$ vs E for ^{56}Fe. References to data (Lu et al, Dilg et al, Katsanos et al, Iljinov et al) and the actual data values are given in Appendix C.

counting and high lying data from Ericson fluctuation (17-23 MeV) are well described. Similarly, as can be seen from Fig. 4.4 the spin-cutoff factors are also well described; $\sigma_J(E) \sim 3.2 - 4.5$ for $E = 4 - 20\,MeV$. The calculated state densities are well represented by the LLC Fermi gas form as shown in Fig. 4.5 and the deduced (a, Δ) values, given in Table 4.12, are in close agreement with values due to Lu et al who used the charge particle data.

4.3.3 Nucleus ^{59}Co

The low-energy data which is used in fixing the reference energy are given in Table 4.13. Also shown in the table are E_{ref}, J^{π}_{ref} and N_{ref} values and with these values,

Table 4.13 Low energy data for reference energy calculation

E (MeV)	J^{π}	Ref
0.0	$7/2^-$	[Nu-83]
1.099	$3/2^-$	[Nu-83]
1.190	$9/2^-$	[Nu-83]
1.292	$3/2^-$	[Nu-83]
1.434	$1/2^-$	[Nu-83]
1.460	$11/2^-$	[Nu-83]
1.482	$5/2^-$	[Nu-83]
1.745	$7/2^-$	[Nu-83]
2.062	$7/2^-$	[Le-78]
2.088	$5/2^-$	[Nu-83]
$E_{ref} = 2.088\ MeV$		$J^{\pi}_{ref} = 5/2^-$
	$N_{ref} = 68$	

the GS energy is calculated, with a trial value of G, using the method outlined in Sect. 4.2.2. The value of G is varied such that the total level density $I_\ell(E)$ at $E = 10\ MeV$ becomes close to the values obtained from the experimental

(proton resonance) data compiled by Iljinov et al (Table C.7) which is $3000 \pm 900\, MeV^{-1}$. With $G = 0.339\, MeV$ the calculated value of $I_\ell(E)$ at 10 MeV is 3045 MeV^{-1}. The state and spin-cutoff variances (σ^2_V, $\sigma^2_{V;J_z^2}$) and the centroid shifts $\epsilon_{V;J_z^2}$ are calculated with $G = 0.339\, MeV$. With these variances and centroid shifts $I(E)$, $I_\ell(E)$ and $\sigma_J(E)$ are calculated at various energies using the procedures given in Sect. 4.2.6 and the results are compared with data in Figs. 4.7, 4.4. It is seen from Fig. 4.7 that the calculations extrapolate the densities from 10 MeV well upto 20 MeV. The calculated spin-cutoff factors (Fig. 4.4) are somewhat smaller (say by 20%) than the experimental values. The $I(E)$ is well represented by LLC Fermi gas form with $(a, \Delta) = (5.84\, MeV^{-1}, -0.74\, MeV)$ as shown in Fig. 4.5 and the deduced a values, as can be seen from Table 4.14 are somewhat smaller than the Lu et al and Dilg et al values.

Table 4.14 Fermi gas parameters

Nucleus	Lu et al		Dilg et al		Present Calculation	
	a (MeV^{-1})	Δ (MeV)	a (MeV^{-1})	Δ (MeV)	a (MeV^{-1})	Δ (MeV)
^{59}Co	6.20	−0.80	6.31	−0.47	5.84*	−0.74*
					5.77@	−0.74@

* for Lang LeCouteur Fermi gas form @ for back shifted Fermi gas form

4.3.4 Nucleus ^{60}Co

Complete low-energy data for ^{60}Co nucleus is available only upto 0.79 MeV [Nu-86b]. As this energy is extremely low, it is not good to consider this energy to be the reference energy. Therefore in this case a different prescription (as

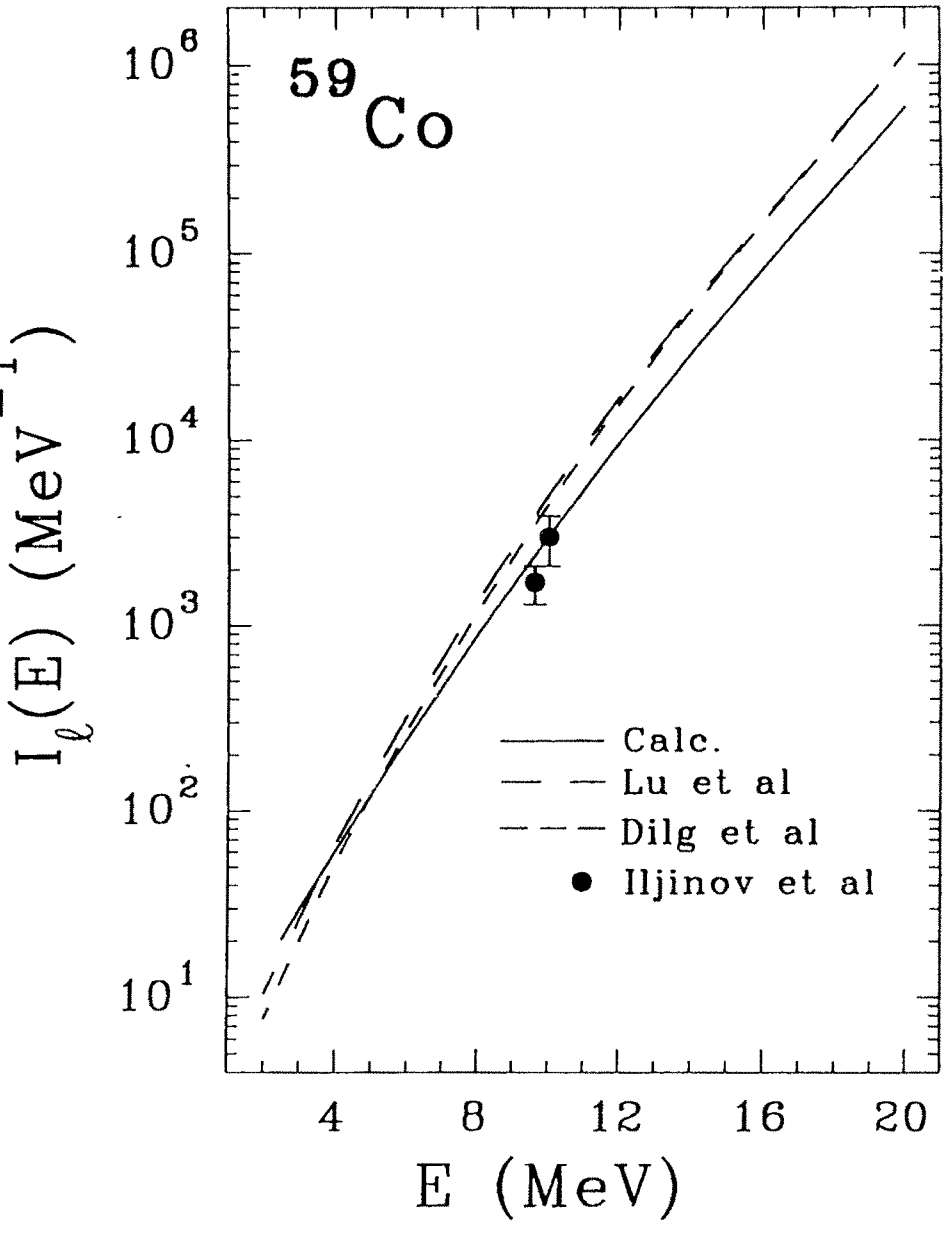

Fig. 4.7 Total level density $I_\ell(E)$ vs E for ^{59}Co. References to data (Lu et al, Dilg et al, Iljinov et al) and the actual data values are given in Appendix C.

compared to the method outlined in Sect. 4.2.2 is used) for fixing the reference energy. Using the Dilg et al data for level densities (Table C.11), at 4 MeV the total number of positive parity states $N^{+}(E_{ref} = 4\,MeV)$ is determined to be 1796. Starting with a value of G, the reference energy $(\overline{E}_{ref})$ is determined using $N^{+}(E_{ref})$ value. The value of G is then varied to reproduce the $I_{\ell}(E)$ value of Dilg et al at 8 MeV excitation $(I_{\ell}(E = 8\,MeV) = 7337\,MeV^{-1})$ and also the neutron resonance density at the resonance energy 7.491 MeV $(I_{\ell}(E = 7.491\,MeV) = 4389 \pm 627\,MeV^{-1})$. To get agreements it is found that a rather low value (compared to $20/A$ MeV) of G has to be used. As this is not proper (G should be normally $25/A$ MeV), the value of G is fixed to be $G = 0.31\,MeV$. Then with the above described method of fixing the reference energy, the $I_{\ell}(E)$ at $E = 8\,MeV$, $7.491\,MeV$ are found to be smaller by a factor 2 and at higher energies by a factor of $3 - 4$ (see the inset to Fig. 4.8). In order to produce satisfactory agreements, the calculated ground state has to be moved up by 1 MeV. The results obtained for $I_{\ell}(E)$, $I(E)$ and $\sigma_{J}(E)$ with $G = 0.31\,MeV$ by the above mentioned correction for GS location, are shown in Figs. 4.8, 4.4.

The source of error in locating properly the GS could be that there is a back shifting as we are using SDI for an odd-odd nucleus. Alternatively this may be due to the fact that level densities at low-energies are quite high for odd-odd nuclei compared to its even-even or odd-A neighbor and with SDI it may not be possible to reproduce these densities. It is worth pointing out that ^{60}Co is the only odd-odd nucleus that is so far analyzed using SAT-LSS [3]. The problems that can be encountered when dealing with odd-odd nuclei should

[3]Behkami and Huizenga [Be-73], in their analysis of fp - shell level density and spin-cutoff factor data using Fermi gas (NIP) theory with pairing, also considered the same set of nuclei listed in Table 4.1 but 'without' ^{60}Co nucleus.

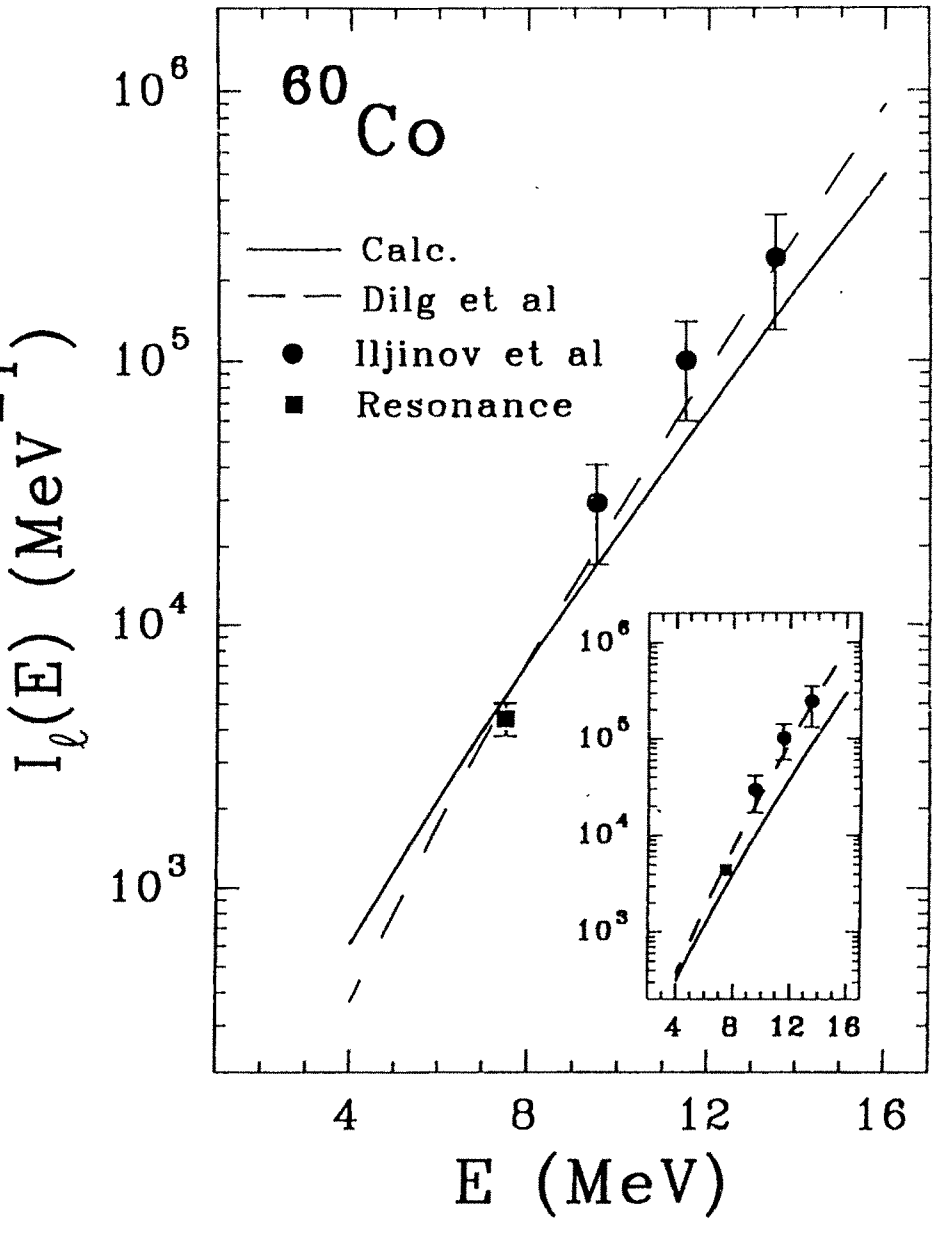

Fig. 4.8 Total level density $I_\ell(E)$ vs E for ^{60}Co. References to data (Dilg et al, Iljinov et al, Resonance) and the actual data values are given in Appendix C. The results shown in the inset figure correspond to the calculation where the ground state is not moved (text gives details).

be explored further.

It can be seen from Figs. 4.8, 4.4, the level densities and spin-cutoff factors for ^{60}Co are well described by the IP theory (level densities are calculated upto 16 MeV). The calculated state densities ($I(E)$) are well represented by the Fermi gas forms as shown in Fig. 4.5. The deduced (a, Δ) values with LLC Fermi gas form are not compatible, as shown in Table 4.15, with Dilg et al values obtained by fitting the low-energy data and the neutron resonance data.

Table 4.15 Fermi gas parameters

Nucleus	Dilg et al		Present Calculation	
	a (MeV^{-1})	Δ (MeV)	a (MeV^{-1})	Δ (MeV)
^{60}Co	6.86	−2.16	5.98*	−3.79*
			5.99@	−3.53@

* for Lang LeCouteur Fermi gas form @ for back shifted Fermi gas form

4.3.5 Nucleus ^{60}Ni

For ^{60}Ni nucleus there is complete low-energy data [Le-78] upto 4.007 MeV, however there are several levels between 3.32 − 4.01 MeV for which the spins and parities are not assigned as can be seen from Table 4.16. In principle one can use, 3.318 MeV level as reference energy as all levels below are identified with J^{π} values assigned. As we are dealing with an even-even nucleus, for these the level densities at low-energies being low, it is always better to use as high a reference energy as possible. Therefore all the levels upto 4.007 MeV shown in Table 4.16 are used but with degeneracies assigned to levels with no J^{π} assignments by using the so called information theory method [Sm-87].

According to the information theory the total number of states $I^{\pi}(E)dE$ at energy E is given by,

$$I^{\overline{\pi}}(E)dE = \frac{\sum_{\substack{J\,(\text{known } J'\text{s} \\ \text{or all } J'\text{s}),\, \pi = \overline{\pi}}} (2J+1)P_{J\pi}}{\sum_{\substack{J\,(\text{known } J'\text{s} \\ \text{or all } J'\text{s}),\, \pi}} P_{J\pi}}$$

$$P_{J\pi} = C_J P_{\pi}$$

$$C_J = \frac{(2J+1)}{\sqrt{8\pi}\sigma_J^3} exp\, -\frac{(J+1/2)^2}{2\sigma_J^2}$$

$$P_{\pi} = 1 \quad \text{desired parity}$$

$$P_{\pi} = \tfrac{1}{2} \quad \text{for unknown parity}$$

$$P_{\pi} = 0 \quad \text{for opposite parity .} \qquad (4.3)$$

In applying (4.3), it should be kept in mind that J-summation is over the known J's if some J assignmments are known and otherwise it is over all J's (i.e. $J = 0$ to ∞). Eq. (4.3) is applied with $\sigma_J = 3$ which is a typical value for ^{60}Ni at low-energies as can be seen from Fig. 4.4. The final reference energy is given in Table 4.16 and with this reference energy the GS is calculated using a trial value for G and the method outlined in Sect. 4.2.2. The neutron resonance data (Table C.13) is found to give a value of $G < 0.3$ (much lower than $20/A\ MeV$) and therefore a search for a value of G (not much lower than $20/A\ MeV$) is made which gives overall good description of $I_\ell(E)$ data from 4 $-$ 24 MeV and the value found is $G = 0.31\ MeV$. The calculated $I_\ell(E)$, $I(E)$ and $\sigma_J(E)$ are compared with data in Figs. 4.9, 4.4. The ^{60}Ni nucleus is the only nucleus in our set that has level density data from all the four sources mentioned in Sect. 4.2.2. As can be seen from Fig. 4.9, the calculations

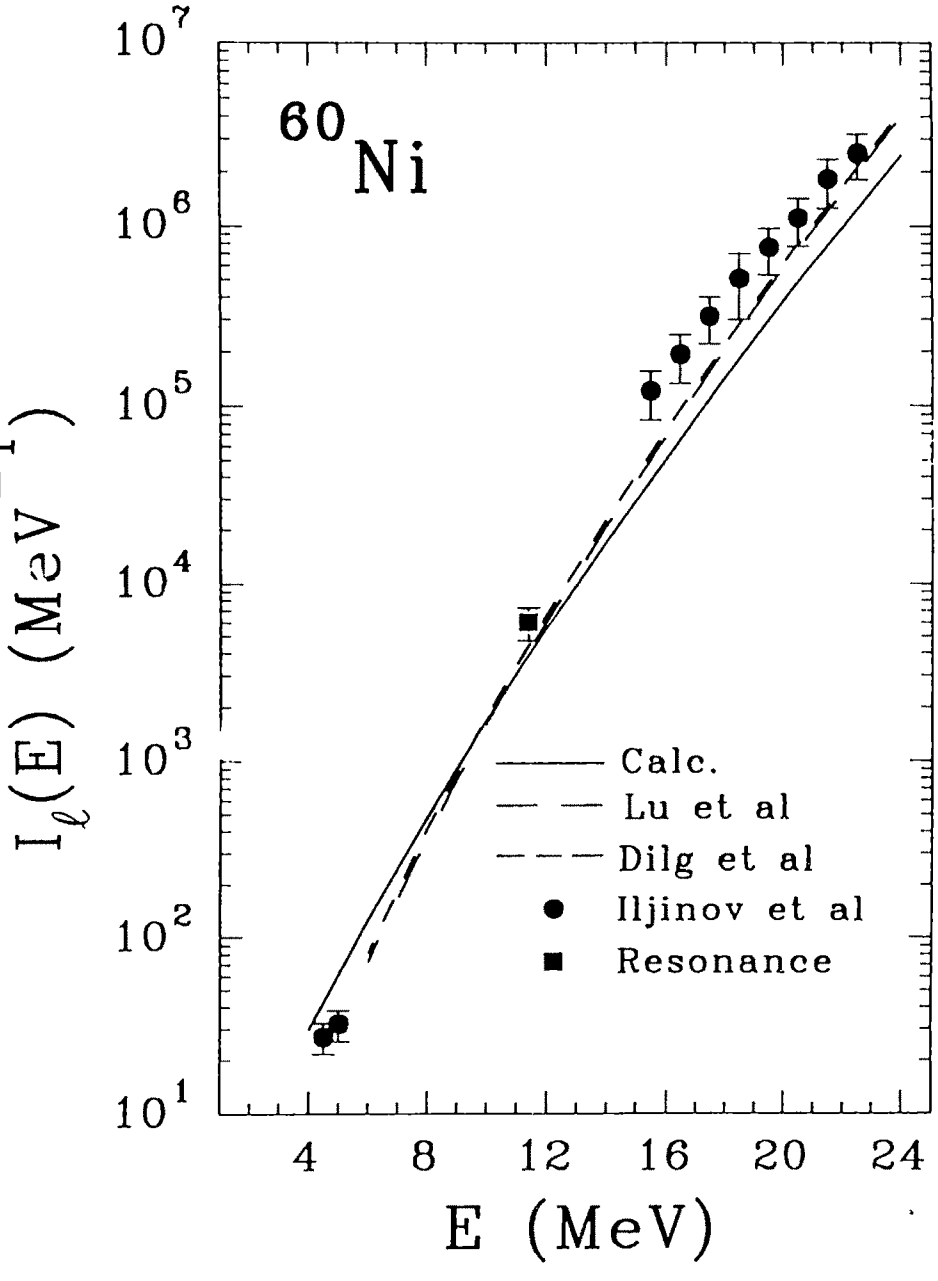

Fig. 4.9 Total level density $I_\ell(E)$ vs E for ^{60}Ni. References to data (Lu et al, Dilg et al, Iljinov et al, Resonance) and the actual data values are given in Appendix C.

with $G = 0.31\ MeV$ describe the data in the $4 - 24\ MeV$ energy range. The deviations at energies $> 16\ MeV$ are not more than a factor 2. The calculated spin-cutoff factor values (Fig. 4.4) are somewhat smaller than data values. The results for ^{60}Ni confirm that the IP theory describes the data in a wide energy range.

Table 4.16 Low energy data for reference energy calculation

E (MeV)	J	π	$I^+(E)dE$	Ref
0.0	0	+	1	[Le-78]
1.333	2	+	5	[Le-78]
2.159	2	+	5	[Le-78]
2.285	0	+	1	[Le-78]
2.506	4	+	9	[Le-78]
2.626	3	+	7	[Le-78]
3.120	4	+	9	[Le-78]
3.124	2	+	5	[Le-78]
3.186	3	+	7	[Le-78]
3.194	1	+	3	[Le-78]
3.269	2	+	5	[Le-78]
3.319	0	+	1	[Le-78]
3.381	unknown	unknown	3.74	[Le-78]
3.394	2	+	5	[Le-78]
3.533	0	+	1	[Le-78]
3.588	0	+	1	[Le-78]
3.620	unknown	unknown	3.74	[Le-78]
3.623	unknown	unknown	3.74	[Le-78]
3.671	4	+	9	[Le-78]
3.700	unknown	unknown	3.74	[Le-78]
3.731	unknown	unknown	3.74	[Le-78]
3.736	2	+	5	[Le-78]
3.738	unknown	unknown	3.74	[Le-78]
3.741	unknown	unknown	3.74	[Le-78]
3.871	unknown	unknown	3.74	[Le-78]
3.875	2	+	5	[Le-78]
3.887	unknown	unknown	3.74	[Le-78]
3.895	unknown	unknown	3.74	[Le-78]
3.925	3	+	7	[Le-78]
4.007	2	+	5	[Le-78]

$E_{ref} = 4.007\ MeV$ $\qquad$ $J^{\pi}_{ref} = 2^+$

$N_{ref} = 133.5$

Once again the state density $I(E)$ is well represented by LLC Fermi gas forms as can be seen from Fig. 4.5. The deduced (a, Δ) values are somewhat smaller than Lu et al (from charge particle spectra) and Dilg et al values, as shown in Table 4.17 but yet the calculated $I(E)$ is quite close to Lu et al and Dilg et al curves (Fig. 4.5).

Table 4.17 Fermi gas parameters

Nucleus	Lu et al		Dilg et al		Present Calculation	
	a (MeV^{-1})	Δ (MeV)	a (MeV^{-1})	Δ (MeV)	a (MeV^{-1})	Δ (MeV)
^{60}Ni	6.40	1.30	6.42	1.14	5.82*	0.22*
					5.84@	0.51@

* for Lang LeCouteur Fermi gas form @ for back shifted Fermi gas form

4.3.6 Nucleus ^{63}Cu

The low-energy data for fixing the reference energy is taken from [Nu-91],

Table 4.18 Low lying data for reference energy calculation

E (MeV)	J^π	Ref
0.0	$3/2^-$	[Nu-91]
0.670	$1/2^-$	[Nu-91]
0.962	$5/2^-$	[Nu-91]
1.327	$7/2^-$	[Nu-91]
1.412	$5/2^-$	[Nu-91]
1.547	$3/2^-$	[Nu-91]
1.861	$7/2^-$	[Nu-91]
2.011	$3/2^-$	[Nu-91]
2.081	$5/2^-$	[Nu-91]
2.093	$7/2^-$	[Nu-91]
2.208	$9/2^-$	[Nu-91]
2.337	$5/2^-$	[Nu-91]
$E_{ref} = 2.337\ MeV$		$J^\pi_{ref} = 5/2^-$
	$N_{ref} = 74$	

With the (E_{ref}, J^{π}_{ref}, N_{ref}) given in the table and a trial value of G the GS energy is determined. Then G is varied to get best possible description of data. An attempt to fix the value of G using the proton resonance data $I_\ell(E) = 2100 \pm 600\, MeV^{-1}$ at $E = 8.6 MeV$ gives a value $G < 0.27\, MeV$ (note that $25/A = 0.397$ for ^{63}Cu) which is not in the acceptable range (this value of G violates the conditions laid down in Sect. 4.2.6 for the goodness of a calculation) and also with $G < 0.27\, MeV$ the $I_\ell(E)$ data above 10 MeV is not well described. With $G = 0.317$ MeV a reasonable description of data is obtained and the corresponding results are shown in Fig. 4.10 (labelled ^{63}Cu (a)). However if the resonance data has to be well represented and also that the description of $I_\ell(E)$ data beyond 10 MeV has to be good then one has to change the $\overline{\Delta}_{fp-g_{9/2}}$ spacing. By decreasing $\overline{\Delta}_{fp-g_{9/2}}$ spacing from 6.53 MeV to 4.53 MeV (given in Table 4.2) but still using $G = 0.317\, MeV$, one gets excellent agreement with data as shown in Fig 4.10 (labelled ^{63}Cu (b)). The decomposition of density into $S = 0$ and $S = 2$ parts clearly shows (Table 4.8) that the $S = 2$ densities dominate over the $S = 0$ densities in this case and therefore ^{63}Cu (b) calculations cannot be considered to be proper calculations. It is possible that most of the $S = 2$ intensity may be coming from excitation into $g_{9/2}$ orbit and then the calculations can be considered acceptable. Altenatively from the ^{63}Cu (b) results one can argue that the decrease in $\overline{\Delta}_{fp-g_{9/2}}$ may be a renormalization effect as we are restricting to 8-orbits. Thus the ^{63}Cu example shows the deficiencies of the choices made regarding s.p. orbits, their s values and $\overline{\Delta}$ spacings for $A > 60$ nuclei. One can resolve these puzzles by performing 10-orbit calculations (by including $2d_{5/2}$ and $1g_{7/2}$ orbits).

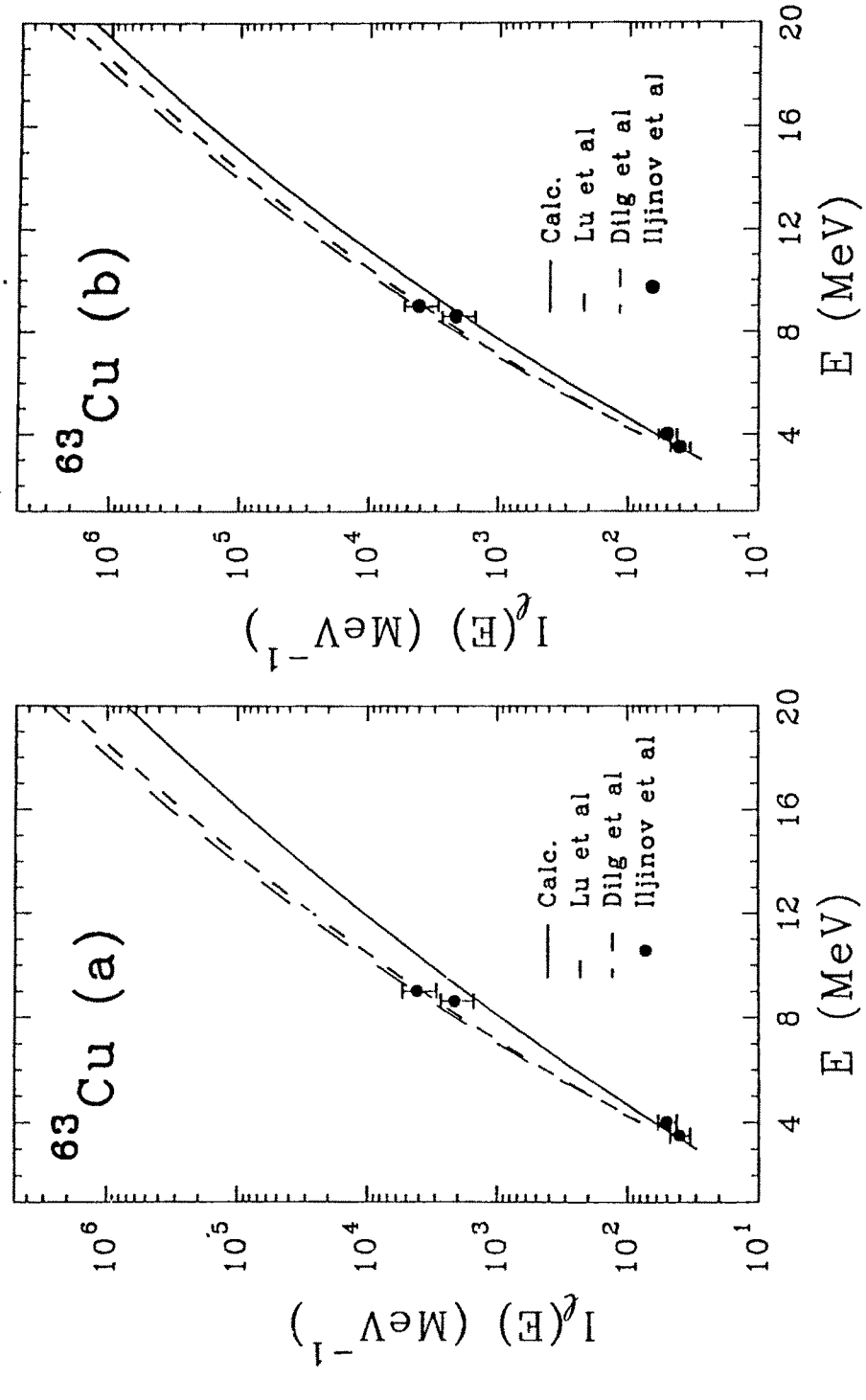

Fig. 4.10 Total level density $I_\ell(E)$ vs E for ^{63}Cu. References to data (Lu et al, Dilg et al, Iljinov et al) and the actual data values are given in Appendix C. The ^{63}Cu (a) and ^{63}Cu (b) calculations are described in the text.

4.3.7 Summary of 8-orbit calculations

For the first time, for a series of fp-shell nuclei, systematic calculations for level densities, state densities and spin-cutoff factors are performed using SAT-LSS (which is a IP theory [4]) and compared with data in Sects. 4.3.1 - 4.3.6. It is seen from Sect. 4.3, the description of the data is excellent for the three nuclei $\{^{55}Mn,\ ^{56}Fe,\ ^{59}Co\}$ and satisfactory for the two nuclei $\{^{60}Co,\ ^{60}Ni\}$. The calculations determine the SDI strength 'G' to be $G \sim 20/A\ MeV$. It is noted that the resulting spreading variances in $S = 0$ case are in general smaller compared to the variances produced by 'renormalized' effective fp-shell interactions. The ^{63}Cu example demonstrates that the 8-orbit calculations have

[4]Starting from Bethe's $exp\sqrt{aE}$ Fermi gas form for level densities, besides deriving various modifications of the Bethe form mainly via various parametrization of the level density parameter 'a' and back shifting parameter 'Δ' [Ig-83, Ka-80; Appendix C], inclusion of pairing via a temperature dependent gap equation [Hu-72, Be-73; Appendix C] and collective effects via a convolution which gives enhancement of level densities by collective enhancement factor given by the partition function of the collective hamiltonians [Ig-83, Ar-91, Ko-93b], there are various attempts to develop a interacting particle level density theory. They are: (i) via Casimir operators of groups as done in the case of Wigner SU(4) by Bloch [Bl-54], Elliott $SU(3)$ by Kanestrom [Ka-66a, Ha-83] and single j - shell pairing [Pa-93]; (ii) employing the CLT results of SAT as given in Chapter 2, a preliminary attempt in this direction is due to Ayik and Ginnochio [Ay-74b] and a more elaborate study is due to Grimes and collabortators [Gr-83] (these studies suffer from the problems mentioned in the beginning of Sect. 3.1). In addition also there is [Ha-82b] the phenomenological version of the theory given in Sect. 3.1; (iii) development of a theory analogous to what was described in Sect. 3.1 but employing a GOE to represent interactions (i.e. $V(2)$) and this work is due to Sato and Yashida [Sa-87a]. It should be noted that GOE is not a model for densities and it is good only for fluctuations. However extension of this work by Pluhar and Weidenmuller [Pl-88], where ensembles similar to what was described in Appendix A are considered but once again by representing the block matrices by GOE, is of importance. The results of this work combined with the model in Appendix A might yield a usable theory for dealing with the important problem of $S = 0 \oplus 2$ mixing (in fact for $S = 0 \oplus 2 \oplus 4 \oplus ....$ mixing) in SAT-LSS; (iv) the so called static path approximation (SPA) due to Bertsch and others [La-88, Al-93] which makes use of the Hubbard-Stratonovich transformation and ideally suited for P + Q.Q interaction. Though this approach is promising, so far no data analysis is carrried out using this method; (v) the Monte Carlo (path integral) method, which is also based on the Hubbard-Stratonovich linearization, for the shell model as being developed by Koonin and collaborators [Jo-92, Ko-94d]. The studies using this method are so far restricted to $0\hbar\omega$ spaces.

problems when applied to $A > 60$ nuclei. It appears that the spectroscopic space has to be enlarged by opening up $(2d_{5/2}, 1g_{7/2})$ orbits. Because of this, in the present section $\{^{62}Ni, ^{65}Cu\}$ nuclei are not analyzed although they are in the selected set given in Table 4.1. The results of the 10-orbit calculations for ^{62}Ni and $^{63,65}Cu$ nuclei are described in the following section.

4.4 Level Density Calculations for fp-shell Nuclei : 10-Orbit Results

Results of ten orbit calculations, with $(2d_{5/2}, 1g_{7/2})$ orbits added to the eight orbits considered in the previous section, for the three nuclei ^{62}Ni, $^{63,65}Cu$ are reported in this chapter. Expansion of the single particle space indeed cures the problems for $A > 60$ nuclei that are highlighted in the previous section with ^{63}Cu example. The ten orbit results are in good agreement with data as can be seen from Sects. 4.4.2 - 4.4.4 ahead. Sect. 4.4.1 gives the choice of s values, single particle energies and centriod separation of unitary orbits and other calculational details.

4.4.1 Choice of s values, single particle energies and centroid separations

Choice of s values

The orbits $(2d_{5/2}, 1g_{7/2})$ are added so that the density at $E > 10\,MeV$ grows and with this, with a reasonable value of G (strength of SDI) and keeping $S = 0$ description to be dominant upto and above E_{ref}, the data is well explained for the three nuclei ^{62}Ni, $^{63,65}Cu$ as can be seen from Sect. 4.4.2 - 4.4.4. The important question that one has to face is that of the s value for the

$2d_{5/2}$, $1g_{7/2}$ orbits. One possible choice is to assign $\bar{s} = 2$ for the three orbits ($1g_{9/2}$, $2d_{5/2}$, $1g_{7/2}$) with $\bar{s} = 0$ and 1 for (ds) and (fp) orbits respectively as

Table 4.19 Unitary orbits for spreading variance calculations

UOV #	Spherical orbits	s value	symbol
#1	$d_{5/2}$, $s_{1/2}$, $d_{3/2}$	0	Λ_{-1}
#2	$f_{7/2}$, $p_{3/2}$, $f_{5/2}$, $p_{1/2}$	1	Λ_0
#3	$g_{9/2}$	2	Λ_1
#4	$d_{5/2}$, $g_{7/2}$	3	Λ_2

Table 4.20 Class structures (for $+ve$ parity states in ^{62}Ni and $-ve$ parity states in $^{63,65}Cu$). In the last three columns, the numbers in the first row for each nucleus and each class correspond to the ratio $\sigma^2_{\mathbf{V}}/\sigma^2_{\mathbf{V}:J^2_Z}$ and the number in the second row give the numbers of UON configurations[†].

S	Class Structure	Class #	^{62}Ni	^{63}Cu	^{65}Cu
0	$(\Lambda_0)^{m_p}(\Lambda_0)^{m_n}$	#1	1.11	1.11	1.12
			63	63	45
2	$(\Lambda_0)^{m_p}(\Lambda_0)^{m_n-2}(\Lambda_1)^{2_n}$	#2	1.07	1.07	1.07
			81	81	63
	$(\Lambda_0)^{m_p}(\Lambda_{-1})^{-1_n}(\Lambda_0)^{m_n}(\Lambda_1)^{1_n}$	#3	1.07	1.07	1.07
			126	126	90
	$(\Lambda_0)^{m_p}(\Lambda_{-1})^{-2_n}(\Lambda_0)^{m_n+2}$	#4	1.07	1.07	1.06
			135	135	81
	$(\Lambda_0)^{m_p-1}(\Lambda_1)^{1_p}(\Lambda_0)^{m_n-1}(\Lambda_1)^{1_n}$	#5	1.07	1.07	1.07
			64	72	54
	$(\Lambda_0)^{m_p-1}(\Lambda_1)^{1_p}(\Lambda_{-1})^{-1_n}(\Lambda_0)^{m_n+1}$	#6	1.07	1.07	1.07
			96	108	72
	$(\Lambda_0)^{m_p-2}(\Lambda_1)^{2_p}(\Lambda_0)^{m_n}$	#7	1.07	1.07	1.07
			49	56	40
	$(\Lambda_{-1})^{-1_p}(\Lambda_0)^{m_p+1}(\Lambda_0)^{m_n-1}(\Lambda_1)^{1_n}$	#8	1.07	1.07	1.08
			144	144	108
	$(\Lambda_{-1})^{-1_p}(\Lambda_0)^{m_p+1}(\Lambda_{-1})^{-1_n}(\Lambda_0)^{m_n+1}$	#9	1.08	1.07	1.08
			216	216	144
	$(\Lambda_{-1})^{-1_p}(\Lambda_0)^{m_p}(\Lambda_1)^{1_p}(\Lambda_0)^{m_n}$	#10	1.07	1.07	1.07
			126	126	90
	$(\Lambda_{-1})^{-2_p}(\Lambda_0)^{m_p+2}(\Lambda_0)^{m_n}$	#11	1.08	1.08	1.08
			189	189	135

Table 4.20 Cont'd

S	Class Structure	Class #	^{62}Ni	^{63}Cu	^{65}Cu
3	$(\Lambda_0)^{m_p}(\Lambda_0)^{m_n-2}(\Lambda_1)^{1_n}(\Lambda_2)^{1_n}$	#12	1.07	1.07	1.07
			81	81	63
	$(\Lambda_0)^{m_p}(\Lambda_{-1})^{m_n-1}(\Lambda_2)^{1_n}$	#13	1.07	1.07	1.07
			126	126	90
	$(\Lambda_0)^{m_p-1}(\Lambda_1)^{1_p}(\Lambda_0)^{m_n-1}(\Lambda_2)^{1_n}$	#14	1.07	1.07	1.07
			64	72	54
	$(\Lambda_0)^{m_p-1}(\Lambda_2)^{1_p}(\Lambda_0)^{m_n-1}(\Lambda_1)^{1_n}$	#15	1.07	1.07	1.07
			64	72	54
	$(\Lambda_0)^{m_p-1}(\Lambda_2)^{1_p}(\Lambda_{-1})^{-1_n}(\Lambda_0)^{m_n+1}$	#16	1.07	1.07	1.07
			96	108	72
	$(\Lambda_0)^{m_p-2}(\Lambda_1)^{1_p}(\Lambda_2)^{1_p}(\Lambda_0)^{m_n}$	#17	1.07	1.07	1.07
			49	56	40
	$(\Lambda_{-1})^{-1_p}(\Lambda_0)^{m_p+1}(\Lambda_0)^{m_n-1}(\Lambda_2)^{1_n}$	#18	1.07	1.07	1.08
			144	144	108
	$(\Lambda_{-1})^{-1_p}(\Lambda_0)^{m_p}(\Lambda_2)^{1_p}(\Lambda_0)^{m_n}$	#19	1.07	1.10	1.07
			126	126	90
4	$(\Lambda_0)^{m_p}(\Lambda_0)^{m_n-2}(\Lambda_2)^{2_n}$	#20	1.07	1.07	1.07
			81	81	63
	$(\Lambda_0)^{m_p-1}(\Lambda_2)^{1_p}(\Lambda_0)^{m_n-1}(\Lambda_2)^{1_n}$	#21	1.07	1.07	1.07
			64	72	54
	$(\Lambda_0)^{m_p-2}(\Lambda_2)^{2_p}(\Lambda_0)^{m_n}$	#22	1.07	1.07	1.07
			49	56	40

† In the table whenever Λ_{-1} is not shown, it implies that Λ_{-1} orbit is full. Similarly Λ_0, Λ_1 and Λ_2 orbits are not shown whenever they are empty.

in the previous section. Let us denote ds, fp and ($1g_{9/2}$, $2d_{5/2}$, $1g_{7/2}$,) orbits as unitary orbits $\overline{\Lambda}_{-1}$, $\overline{\Lambda}_0$,$\overline{\Lambda}_1$ respectively. With this choice, the calculated density is not found to be acceptable as $\bar{S} = 2$ intensity even at E_{ref} and below is nearly 100%. The reason for this is that the $\bar{S} = 2$ class variances become larger by about 20% compared to the corresponding variances without ($2d_{5/2}$, $1g_{7/2}$) orbits. This then leads to the natural choice of $s = 2$ for $1g_{9/2}$ as before and $s = 3$ for ($2d_{5/2}$, $1g_{7/2}$) orbits. This is consistent with the fact that $1g_{9/2}$ orbit is well separated from ($2d_{5/2}$, $1g_{7/2}$) orbits to form the magic number 50. With this choice there are four unitary orbits (UOV) for variance calculations as given in Table 4.19. Then for example, a $S = 2$ class $(\overline{\Lambda}_0)^{-2p}$

$(\overline{\Lambda}_1)^{2p} \rightarrow (\Lambda_0)^{-2p}\,(\Lambda_1)^{2p} \oplus (\Lambda_0)^{-2p}\,(\Lambda_1)^{1p}\,(\Lambda_2)^{1p} \oplus (\Lambda_0)^{-2p}\,(\Lambda_2)^{2p}$ with $S = 2$, 3 and 4 respectively. Thus we are led to $S = 4$ calculations in the 10-orbit case. The corresponding classes (one $S = 0$, ten $S = 2$, eight $S = 3$ and three $S = 4$) are given in Table 4.20.

Single particle energies and choice of centroid separations

The s.p. energies for the ds, fp and $1g_{9/2}$ orbits are same as in the 8-orbit calculations. The $1g_{7/2}$ orbit energy is chosen to be 4 MeV above the $1g_{9/2}$ orbit and the $2d_{5/2} - 1g_{7/2}$ separation is chosen to be 0.68 MeV as in ^{116}Sn calculations [Bo-85]. With this choice, the resulting traceless single particle energies and the centroid separations (which are referred to as $\overline{\Delta}^{(1)}$ below), are given in Table 4.21. With the centroid separation $\overline{\Delta}^{(1)}$ given below, it is

Table 4.21 Quantum numbers and energies of s.p. orbits

orbit #	s	n	ℓ	j	ϵ_j (MeV)
#1	0	0	2	5/2	−1.838
#2	0	1	0	1/2	−0.968
#3	0	0	2	3/2	3.242
#4	1	0	3	7/2	−2.664
#5	1	1	1	3/2	−0.644
#6	1	0	3	5/2	3.526
#7	1	1	1	1/2	1.366
#8	2	0	4	9/2	0.000
#9	3	1	2	5/2	0.389
#10	3	0	4	7/2	−0.291

$$\overline{\Delta}^{(1)}_{sd-fp} = 11.03\,MeV \quad \overline{\Delta}^{(1)}_{fp-g_{9/2}} = 6.53\,MeV \quad \overline{\Delta}^{(1)}_{g_{9/2}-\{d_{5/2},g_{7/2}\}} = 4.29\,MeV$$

$$\overline{\Delta}^{(2)}_{sd-fp} = 11.03\,MeV \quad \overline{\Delta}^{(2)}_{fp-g_{9/2}} = 5.78\,MeV \quad \overline{\Delta}^{(2)}_{g_{9/2}-\{d_{5/2},g_{7/2}\}} = 3.29\,MeV$$

found that, for ^{62}Ni and ^{63}Cu the calculated densities are usually small by a factor 2 and therefore the $\overline{\Delta}^{(1)}_{fp-g_{9/2}}$ is decreased by 0.75 MeV and $\overline{\Delta}^{(1)}_{g_{9/2}-\{d_{5/2},g_{7/2}\}}$

by 1 MeV and with this choice (denoted as $\overline{\Delta}^{(2)}$ in Table 4.21), together with reasonable value for G, good agreements with data are obtained and also the $S = 0$ description upto and above E_{ref}; in the case of ^{65}Cu, $\overline{\Delta}^{(1)}$ choice is found to be good. The S-decomposition of the densities is given in Table 4.22.

Table 4.22 S-decomposition of state densities. For a given nucleus and a given energy, the four entries are (in MeV^{-1}) for $I^{\pi}_{\ell;S=0}(E)$, $I^{\pi}_{\ell;S=2}(E)$, $I^{\pi}_{\ell;S=3}(E)$ and $I^{\pi}_{\ell;S=4}(E)$ respectively. The parity $\pi = +$ for ^{62}Ni and $\pi = -$ for $^{63,65}Cu$. The $^{65}Cu(a)$ and $^{65}Cu(b)$ are described in Sect. 4.4.4.

E (MeV)	^{62}Ni	^{63}Cu	$^{65}Cu(a)$	$^{65}Cu(b)$
$E^{\dagger}_{ref}$	13	6	2	6
	5	3	5	2
	1	0	1	0
	0	0	0	0
$E^{\dagger}_{res}$	915	422	611	1259
	982	408	2808	2034
	220	92	915	258
	7	3	43	3
16.0	14263	18962	8444	15021
	33048	50868	69794	56811
	10863	18678	31741	12108
	549	1115	2362	342

† For ^{62}Ni, $E_{ref} = 4.055\,MeV$, $E_{res} = 10.597\,MeV$; For ^{63}Cu, $E_{ref} = 2.337\,MeV$, $E_{res} = 8.6\,MeV$; For ^{65}Cu, $E_{ref} = 2.329\,MeV$, $E_{res} = 10.65\,MeV$

Calculational details

The $\sigma^2_V/\sigma^2_{V;J^2_Z}$ ratio is fixed in the following way. The $S = 0$ and $S = 2$ classes in the 8 and 10-orbit calculations are identical. Therefore for these classes the results given in Table 4.7 for the $\sigma^2_V/\sigma^2_{V;J^2_Z}$ ratio are used. For the

$S = 3$ and $S = 4$ classes, the value for the corresponding $S = 2$ classes that has same number of protons and neutrons in $ds(\Lambda_{-1})$ and $fp(\Lambda_0)$ unitary orbits is taken (for example for $(\Lambda_0^{-2_n})$ $(\Lambda_1^{2_n})$, $(\Lambda_0^{-2_n})$ $(\Lambda_1^{1_n})$ $(\Lambda_2^{1_n})$, $(\Lambda_0^{-2_n})$ $(\Lambda_2^{-2_n})$ which have $S = 2$, 3 and 4 respectively, the $\sigma_V^2/\sigma_{V:J_z^2}^2$ is taken to be that of $(\Lambda_0^{-2_n})$ $(\Lambda_1^{2_n})$ class). The final values for all the classes are given in Table 4.20.

For the calculation of NIP densities, the choice that is made for the UON unitary orbits is given in Table 4.23. The number of unitary configurations defined by UON for each nucleus for each of the 22 classes are given in Table 4.20. All other calculational procedures are same as in Sect. 4.2.

Table 4.23 Unitary orbits for NIP calculations

UON #	Spherical orbits	s
#1	$d_{5/2}, s_{1/2}$	0
#2	$d_{3/2}$	0
#3	$f_{7/2}$	1
#4	$p_{3/2}$, $f_{5/2}$, $p_{1/2}$	1
#5	$g_{9/2}$	2
#6	$d_{5/2}, g_{7/2}$	3

4.4.2 Nucleus ^{62}Ni

For ^{62}Ni nucleus there is complete low-energy data [Nu-90] upto 4.055 MeV, however there are several levels between $3.258 - 4.055$ MeV for which the spins and parities are not assigned as can be seen from Table 4.24. In principle it is possible to use 3.258 MeV level as reference energy as all levels below this energy are identified with J^π values assigned. For even-even nuclei, as for these nuclei the level densities at low-energies being low, it is always better to use as high a reference energy as possible. Therefore all the levels upto 4.055 MeV

shown in Table 4.26 are used but with degeneracies assigned to levels with no J and/or π assignments by using information theory method described in Sect. 4.3.5. In applying (4.3) the value of spin-cutoff factor has been taken to be 3.0. The final (E_{ref}, N_{ref} and J^{π}_{ref}) values are given

Table 4.24 Low energy data for reference energy calculation

E (MeV)	J	π	$I^{+}(E)dE$	Ref
0.00	0	+	1	[Nu-90]
1.173	2	+	5	[Nu-90]
2.049	0	+	1	[Nu-90]
2.302	2	+	5	[Nu-90]
2.336	4	+	9	[Nu-90]
2.891	0	+	1	[Nu-90]
3.059	2	+	5	[Nu-90]
3.158	2	+	5	[Nu-90]
3.177	4	+	9	[Nu-90]
3.258	2	+	5	[Nu-90]
3.262	(2,4)	+	6.81	[Nu-90]
3.270	1,2	+	4.14	[Nu-90]
3.277	4	+	9	[Nu-90]
3.370	1,2	+	4.14	[Nu-90]
3.378	unknown	unknown	3.74	[Nu-90]
3.462	1,2,3,4	+	6.07	[Nu-90]
3.486	unknown	unknown	3.74	[Nu-90]
3.500	2	+	5	[Nu-90]
3.519	2	+	5	[Nu-90]
3.523	2,3	+	6.00	[Nu-90]
3.757	3	−	0.00	[Nu-90]
3.844	unknown	unknown	3.74	[Nu-90]
3.849	0,1,2	+	3.71	[Nu-90]
3.853	2	+	5	[Nu-90]
3.860	1,2	+	4.14	[Nu-90]
3.967	unknown	+	7.48	[Nu-90]
3.973	2	+	5	[Nu-90]
3.998	4	+	9	[Nu-90]
4.019	6	+	13	[Nu-90]
4.036	unknown	+	7.48	[Nu-90]
4.055	4	+	9	[Nu-90]
$E_{ref} = 4.055\ MeV$			$J^{\pi}_{ref} = 4^{+}$	
$N_{ref} = 167.2$				

in Table 4.24. With this reference energy data and the unitary orbit control separation as given by $\overline{\Delta}^{(2)}$ in Table 4.21, the GS is calculated using a trial value for G. The level density ($4552\ MeV^{-1}$) at the neutron resonance energy $10.597\ MeV$ is reproduced with $G = 0.305\,MeV$. The values of $\sigma^2_{\mathbf{V}}$, $\sigma^2_{\mathbf{V}:J^2_z}$ and $\epsilon_{\mathbf{V}:J^2_z}$ calculated with $G = 0.305\,MeV$ are 12.8 MeV^2, 11.6 MeV^2 and 0.004 MeV respectively for $S = 0$ configuration, $\sim$ 17 MeV^2, $\sim$ 16 MeV^2 and $\sim$ 0.01 MeV respectively for $S = 1$ configurations, $\sim$ 22 MeV^2, $\sim$ 21 MeV^2 and $\sim$ 0.02 MeV respectively for $S = 2$ configurations, $\sim$ 22 MeV^2, $\sim$ 20 MeV^2 and $\sim$ 0.01 MeV respectively for $S = 3$ configurations, $\sim$ 20 MeV^2, $\sim$ 18 MeV^2 and $\sim$ 0.001 MeV respectively for $S = 4$ configurations. The calculated $I_\ell(E)$, $I(E)$ and $\sigma_J(E)$ are compared with data in Figs. 4.11, 4.4. As can be seen from Fig. 4.11, the calculations with $G = 0.305\,MeV$ describe the data in the $4 - 20\ MeV$ energy range (the Lu et al (b) curve is consistently low compared to the calculated curve). The calculated spin-cutoff factor values (Fig. 4.4) are somewhat smaller than data values at low-energies. The results for ^{62}Ni confirm that the IP theory describes the data in a wide energy range. The state density $I(E)$ is well represented by LLC Fermi gas forms as can be seen from Fig. 4.5. The deduced (a, Δ) values are given in Table 4.25.

Table 4.25 Fermi gas parameters

Nucleus	Lu et al (a)		Lu et al (b)		Dilg et al		Present Calculation	
	a (MeV^{-1})	Δ (MeV)	a (MeV^{-1})	Δ (MeV)	a (MeV^{-1})	Δ (MeV)	a (MeV^{-1})	Δ (MeV)
^{62}Ni	6.40	0.5	6.40	1.30	7.27	1.07	6.44*	0.40*
							6.45@	0.67@

* for Lang LeCouteur Fermi gas form @ for back shifted Fermi gas form

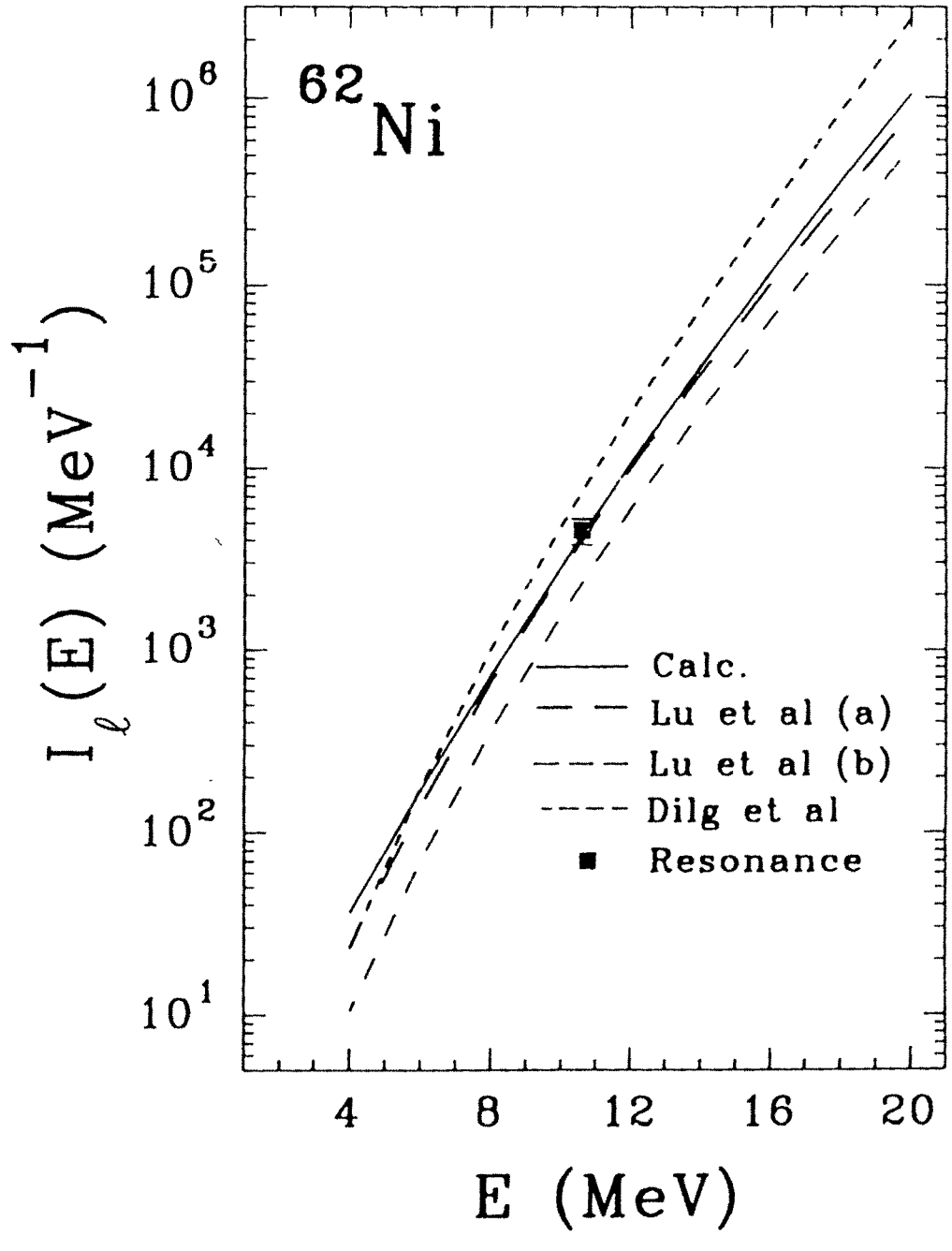

Fig. 4.11 Total level density $I_\ell(E)$ vs E for ^{62}Ni. References to data (Lu et al (a), Lu et al (b), Dilg et al, Resonance) and the actual data values are given in Appendix C.

4.4.3 Nucleus ^{63}Cu

With the low-energy data given in Sect. 4.3.6, centroid separation given by $\overline{\Delta}^{(2)}$ in Table 4.21 and the proton resonance data ($E_{res} = 8.6\,MeV$, $I_\ell(E) = 2100\,MeV^{-1}$) determine the value of G to be 0.305 MeV. Using this deduced value of G the calculated values of $I(E)$, $I_\ell(E)$ and $\sigma_J(E)$ are compared with data in Figs. 4.12, 4.4. Beyond the resonance energy of 8.6 MeV, the calcualted values are found to be lower, by about 40%, compared to data. The spin-cutoff factors change from $\sigma_J(E) = 3$ to 4 as E changes from 4 to 12 MeV while the data values are around 4 with an error of $10 - 20\%$. The Fermi gas fits to the calculated $I(E)$ and the deduced values of (a, Δ) are given in Fig. 4.5 and Table 4.26 respectively.

Table 4.26 Fermi gas parameters

Nucleus	Lu et al		Dilg et al		Present Calculation	
	a (MeV^{-1})	Δ (MeV)	a (MeV^{-1})	Δ (MeV)	a (MeV^{-1})	Δ (MeV)
^{63}Cu	6.60	−0.50	6.24	−0.77	6.44*	−0.32*
					6.45@	−0.06@

* for Lang LeCouteur Fermi gas form @ for back shifted Fermi gas form

Thus ^{62}Ni and ^{63}Cu are reasonably well described by using the centroids separation as given by $\overline{\Delta}^{(2)}$ in Table 4.21. The $\overline{\Delta}^{(1)}$ set is found to give densities to be too low, compared to data, to be acceptable.

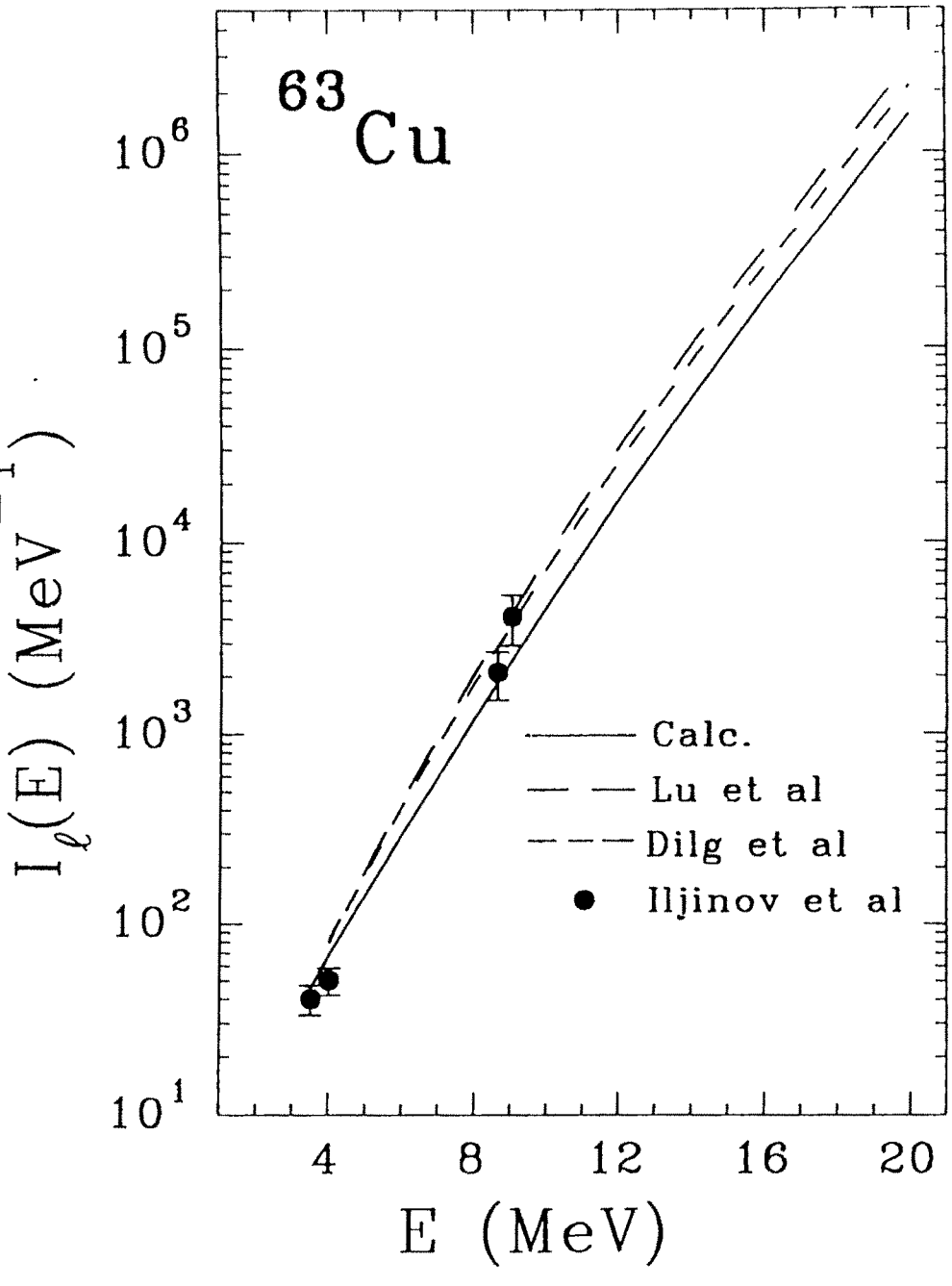

Fig. 4.12 Total level density $I_\ell(E)$ vs E for ^{63}Cu. References to data (Lu et al, Dilg et al, Iljinov et al) and the actual data values are given in Appendix C.

4.4.4 Nucleus ^{65}Cu

The low-energy data for fixing the reference energy is taken from [Nu-86a]. Two sets of calculations are performed for ^{65}Cu. In the first set of calculations, the centroid separations are chosen to be same as in ^{62}Ni and ^{63}Cu cases, i.e. $\overline{\Delta}^{(2)}$ set given in Table 4.21 is used. This set (the corresponding calculation is called ^{65}Cu (a)), the low-energy data given in Table 4.27 and the resonance data ($E_{res} = 10.65\,MeV$, $I_\ell(E_{res}) = 6854 \pm 2056\,MeV^{-1}$) are used to determine the value of G. The deduced value is $G = 0.315\,MeV$ and even with this high value of G (compared to 0.305 MeV used in ^{62}Ni and ^{63}Cu cases), the resonance

Table 4.27 Low lying data for reference energy calculation

E (MeV)	J^π	Ref
0.0	$3/2^-$	[Nu-86a]
0.77	$1/2^-$	[Nu-86a]
1.115	$5/2^-$	[Nu-86a]
1.481	$7/2^-$	[Nu-86a]
1.623	$5/2^-$	[Nu-86a]
1.725	$3/2^-$	[Nu-86a]
2.094	$7/2^-$	[Nu-86a]
2.107	$5/2^-$	[Nu-86a]
2.213	$1/2^-$	[Nu-86a]
2.278	$7/2^-$	[Nu-86a]
2.329	$3/2^-$	[Nu-86a]
$E_{ref} = 2.329\,MeV$		$J^\pi_{ref} = 3/2^-$
	$N_{ref} = 58$	

density is predicted to be $\sim 9000\,MeV^{-1}$ which is just within the error bar of the resonance density $6854 \pm 2056\,MeV^{-1}$. As a consequence, at $E \gtrsim 16\,MeV$ the calculated $I_\ell(E)$ differ from Dilg et al data by a factor 2. However it is in close agreement with Lu et al data as shown in Fig. 4.13. In order to

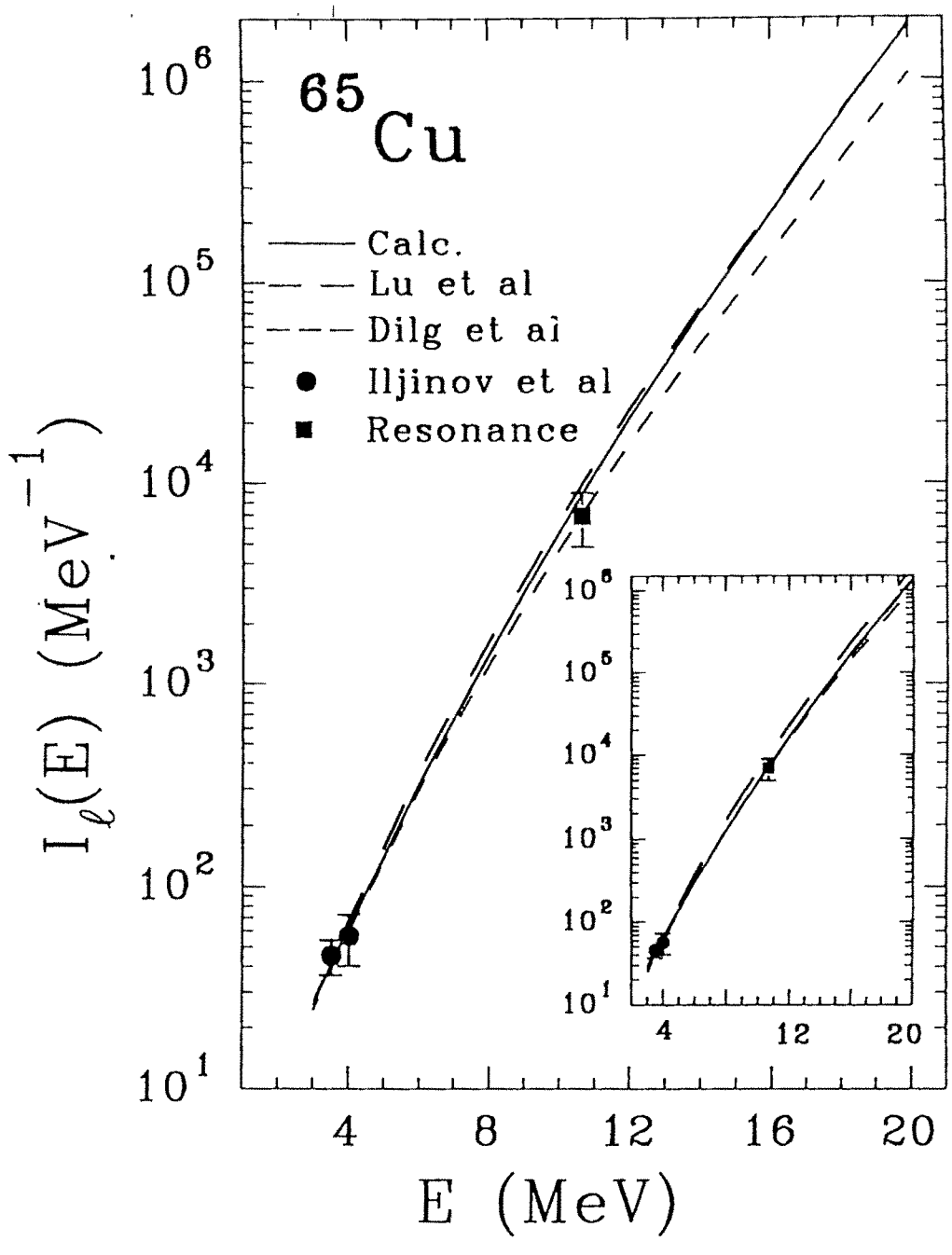

Fig. 4.13 Total level density $I_\ell(E)$ vs E for ^{65}Cu. References to data (Lu et al, Dilg et al, Iljinov et al, Resonance) and the actual data values are given in Appendix C. The results shown in the inset figure correspond to ^{65}Cu (b) calculations described in the text.

reproduce the resonance density value of 6800 MeV^{-1}, one has to use a much larger G value and also the $S = 2$ intensities become much larger than $S = 0$ intensities at low-energies which cannot be accepted. However using a different set (the corresponding calculation is called ^{65}Cu (b)) of centroid separations, as given by the set $\overline{\Delta}^{(1)}$ in Table 4.21, the value of G is determined to be 0.3 MeV. With this the resonance density is reproduced rather well as also Dilg et al data upto 20 MeV. However, here the deviations from Lu at al data is by about 40% as shown in the inset figure of Fig. 4.13. To be consistent with ^{62}Ni and ^{63}Cu calculations, the $^{65}Cu(a)$ results are accepted to be the final results. Therefore for $^{65}Cu(a)$ calculation, the results for $\sigma_J(E)$ vs E are shown in Fig. 4.4 and also the Fermi gas fits are made for $I(E)$ obtained in this case. The deduced values of (a, Δ) are given in Table 4.28 and the fit is shown in Fig. 4.5.

Table 4.28 Fermi gas parameters

Nucleus	Lu et al		Dilg et al		Present Calculation ^{65}Cu (a)	
	a (MeV^{-1})	Δ (MeV)	a (MeV^{-1})	Δ (MeV)	a (MeV^{-1})	Δ (MeV)
^{65}Cu	6.60	−0.50	6.24	−0.77	6.58*	−0 38*
					6.60@	−0.13@

* for Lang LeCouteur Fermi gas form @ for back shifted Fermi gas form

4.5 Summary

First systematic calculations, of level densities and spin-cutoff factors for all nuclei in a given region of the periodic table, in SAT-LSS framework are presented in this chapter with fp-shell nuclei as example. With the 8 - orbit

calculations for the five nuclei ^{55}Mn, ^{56}Fe, ^{59}Co, ^{60}Co, ^{60}Ni (described in Sect. 4.3) and 10 - orbit calculations for the three nuclei ^{62}Ni, ^{63}Cu, ^{65}Cu (described in 4.4), it is clearly demonstrated (as can be seen from Figs. 4.3 - 4.13) that SAT-LSS describes the level densities and spin-cutoff factors data rather well and that it is a powerful tool in analyzing and predicting statistical properties of nuclei. The calculations determine a magnitude parameter of the interaction - the strength G which is found to be $\sim 20/A\ MeV$ for all the nuclei is compatible with the values deduced from low-energy spectroscopy. The theory is seen to provide an excellent extrapolation from the resonance energy ($\sim 8\ MeV$) to $\sim 20\ MeV$ excitation and interpolation between the reference energy ($\sim 3-4\ MeV$) and the resonance energy. The calculated spin-cutoff factors and their energy variations (deriving from $J_Z^2 - \mathbf{V}^2$ correlations) are in good accord with the values deduced from data.